sciendo
Powder Metallurgy Progress, Vol.19 (2019), No.2, p.053-062
http://dx.doi.org/10.1515/pmp-2019-0006

SUPERSOLIDUS SINTERING OF Cr PREALLOYED STEELS BY INDUCTIVE HEATING

C. Gierl-Mayer, M. C. Huemer, H. Danninger, M. Dlapka, G. Stetina, R. Ratzi

Dedicated to the memory of Dr. Gert Leitner (1940-2019), a pioneer of thermal analysis and induction sintering

Abstract
For powder metallurgy products, high density is an essential requirements to obtain maximum mechanical properties. Here, supersolidus liquid phase sintering (SSPLS) is an effective means to attain high sintered density, as known from PM high speed steels. In the present work it is shown that this technique can also be applied to Cr prealloyed low alloy steel grades. Supersolidus sintering through indirect heating requires precise control of temperature and also the atmosphere, to avoid uncontrolled changes of the carbon level. Higher C contents are beneficial here since they enable lower temperatures and result in wider temperature windows for sintering. The temperatures necessary for SSLPS at moderate C levels are fairly high for standard sintering furnaces, therefore induction sintering was studied in this work. It showed that, as was to be expected, also here precise temperature control is required, but for any carbon level tested a sintering temperature could be identified that yielded high sintered density and good shape retention. The high density attained, in combination with the very high temperatures, results in pronounced grain growth, this process no more being inhibited by the presence of pores, which is undesirable but can however be remedied by suitable heat treatment.
Keywords: supersolidus sintering, induction sintering, microstructure

INTRODUCTION

Complex-shaped powder metallurgy precision parts have gained high industrial and economical importance, especially in the automotive industry. Due to the variety of manufacturing methods, alloying technique and alloying elements, the required properties can be tailored specifically, with significantly more flexibility than with wrought steels. The main property that determines the mechanical property is the density level, which typically results from the compacted component. For highly loaded components it is frequently essential to produce PM steels with low to very low residual porosity, which is difficult to obtain by pressing, intolerably high compacting pressures being required. On the other hand, increasing the density can be attained inter alia by activated sintering, in particular liquid phase sintering [1,2].

Christian Gierl-Mayer, Marie-Christine Huemer, Herbert Danninger: Institute of Chemical Technologies and Analytics, TU Wien. Vienna, Austria
Magdalena Dlapka, Gerold Stetina: Miba Sinter Austria GmbH, Dr. Mitterbauer-Str.1, AT-4655 Vorchdorf, Austria
Raimund Ratzi: MIBA AG, AT-4665 Laakirchen, Austria

Liquid phase sintering can be classified in two variants: sintering with a persistent liquid phase, which is present throughout the whole sintering process in virtually the same amount, and on the other hand a transient liquid phase that intermediately appears for a short time [3,4]. For attaining densification during sintering the persistent variant is better suited, as evident from sintering e.g. of hardmetals or W heavy alloys. Supersolidus liquid phase sintering (SPLS) is a special case of liquid phase sintering, first published by Lund and Bala [5]. Thereby an alloy powder, heated to a temperature between the liquidus and the solidus, is used. The liquid is formed inside the particles, and the resulting densifying process can be described as a rapid viscose flow through the effect of capillary forces. [6,7,8].

As typical for SSLPS, an accurate control of the sintering temperature is required to avoid oversintering which occurs in presence of too much liquid and in consequence leads to distortion of the compacts and to undesirable microstructures; nevertheless a critical amount of liquid is necessary to promote full densification [9,10]. Therefore, the application of SSLPS so far has been limited to a few materials, mainly high speed steels [11,12], although studies have been done also with other materials such as e.g. brass [13]. The aim of the present investigation is to show that the SSPLS process can also be adopted to Cr prealloyed low alloy steel grades. For this purpose, sintering of powder compacts was done conventionally in a dilatometer and secondly, because of the fairly high temperatures necessary at moderate C levels, by induction sintering of presintered specimens, inductive heating being better suited for very high temperatures.

Induction sintering, both as a variant of direct sintering or indirectly using a susceptor [14,15], has been studied frequently, in particular for hardmetals, but also for PM steels [16, 17], but so far the industrial applications are very limited, similar as for other “flash” sintering techniques such as microwave sintering. One reason is that sintering involves not only densification and formation of metallic bridges, but also chemical processes such as removal of the “natural” oxygen have to be considered. If however these processes could be separated from the “densification step” and moved into a preceding solid state sintering process, a short-time induction sintering can be expected to perform the required densification without problems from gas-forming processes, and this was investigated here.

EXPERIMENTAL PROCEDURE

The first experiments on Supersolidus Liquid Phase Sintering of chromium containing steels were carried out using a pushrod dilatometer as a minisize, precisely controllable sintering furnace. As a preliminary study, prealloyed powder AstaloyCrM, a water atomized steel powder grade from Höganäs AB, Sweden, was mixed with 1.0 % carbon (natural graphite Kropfmühl UF4) in a turbula mixer for 60 minutes (all concentrations are given in wt%). As typical for prealloyed powders, both alloying elements, chromium (3.0%) and molybdenum (0.5%), were distributed homogeneously in the material. After blending, the powder mix was compacted at 600 MPa to Charpy samples (ISO 5754). The following sintering process was accomplished in a pushrod dilatometer (Netzsch 402) with a heating rate of 10 K/min, subsequent isothermal sintering at 1365°C for 1 hour and cooling once more with a rate of 10 K/min, the atmosphere being rotary pump vacuum (8•10-3 mbar at room temperature and 2•10-2 mbar at sintering temperature). For characterization, the dimensional change, the Archimedes density, the unnotched Charpy impact energy and the Vickers hardness of the sample were measured.

Based on these results, further experiments were performed using induction sintering. Specimens dewaxed/presintered (in fact solid state sintered) in a tube furnace at 1250°C were inductively high temperature sintered for a short time.

AstaloyCrM powders were blended with 0.6, 0.7, 0.8, 0.9, 1.0, 1.1, 1.2 and 1.4% C and once more pressed to Charpy bars at 600 MPa. In the first step, a dewaxing/presintering/deoxidizing step was done as described above in atmosphere N_2-10%H_2 (both purity 5.0). Pieces of the pre-sintered samples were cut, transferred into a graphite crucible and heated with a rate of 400 K/min in a medium frequency induction furnace (pure N_2, quality 5.0) to 1310, 1340, 1370, 1400 and 1430°C. The temperature control was performed by a pyrometer which was placed in such a way that it was possible to measure the temperature on the base plate of the crucible. The samples were isothermally held at these temperatures for 5 min, and then a cooling rate of 600 K/min was adjusted (which could however be maintained only in the higher temperature range). A nitrogen pressure of 800 mbar, slightly below ambient pressure, was necessary to keep the furnace gas tight.

On the sintered specimens, the density was measured through Archimedes' principle (water displacement). Then, cross-sections of the samples were prepared for light microscopic investigations (unetched and etched), and the Vickers hardness, HV30, was measured.

RESULTS AND DISCUSSION

Sintering in the dilatometer

In Table 1 the properties of the conventionally sintered AstaloyCrM+1.0%C (admixed) sample are listed. As shown here, a density of 7.76 g/cm³ could be reached without compromising the dimensional stability, the shape of the bars remaining precisely rectangular. Due to the moderate heating rate (10 K/min) of the dilatometer (tube furnace: 60-100 K/min) which enables a slow, controlled and uniform heat penetration, no gas outbursts occurred; the degassing/deoxidizing process was completed before densification had proceeded so far that the pore channels were closed.

Tab.1. Measured properties (as sintered) of the AstaloyCrM+ 1.0%C impact test bar, sintered in the dilatometer at 1365°C, 10 K/min-60min-10 K/min, vacuum

Sintering Temperature	[°C]	1365
Density	[g/cm³]	7.76
Dimensional Change	[%lin.]	-3.35
Impact energy	[J/cm²]	8.2
Hardness	[HV30]	412

For characterization of the structure, a cross section of the sample was prepared, polished and photographed; (see Figure 1a). The sample is highly dense, just a few, partly small, pores are visible. During SSLPS the grains seem to coarsen a lot, which is not surprising regarding the high temperature and very low porosity (see [18]); the low impact energy can be attributed in part to this coarse microstructure.

For revealing the matrix microstructure, the section was etched with 3% Nital; see Figure 1b. A network of proeutectoid cementite seemed to have been formed at the grain boundaries during SSPLS, in addition to a predominantly bainitic/martensitic

microstructure. This results in quite high values for the Vickers macrohardness (see Table 1) but a low impact energy, the grain coarsening described above enhancing the adverse effect of proeutectoid cementite on the impact behavior.

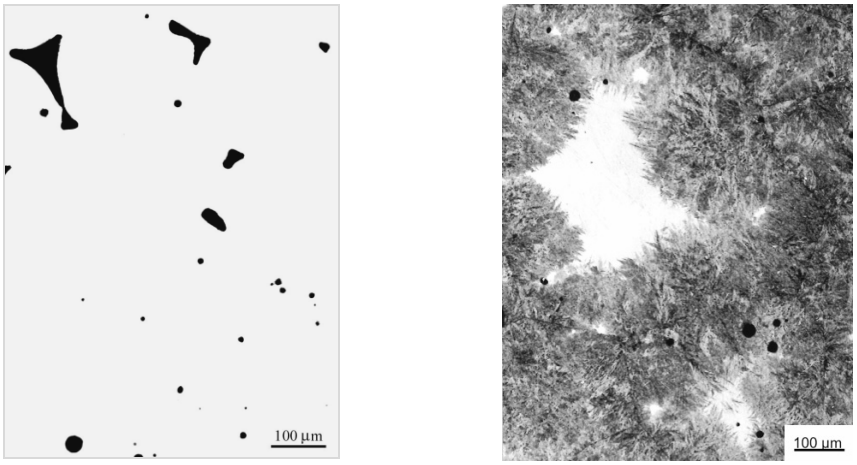

Fig.1. AstaloyCrM+1.0%C, sintered in the dilatometer at 1365°C, 10K/min-60min-10K/min, vacuum; (a) unetched, (b) etched with 3% Nital.

In any case, these preliminary results have shown that by SSLPS, pronounced densification can also be attained with chromium containing low alloy steels, but a subsequent heat treatment step for grain refinement and dissolution of proeutectoid cementite is regarded necessary.

Presintering and final induction sintering

Based on the promising results of the first indirect sintering runs done at 1365°C, the first temperature set for induction sintering was 1370°C. In Figure 2 the different samples containing varying amounts of admixed carbon ranging from 0.6 to 1.4 %C, are shown after the induction sintering step (5 min hold).

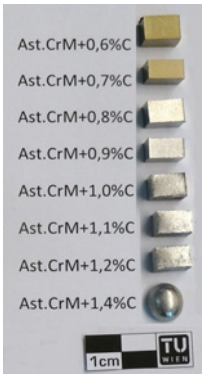

Fig.2. AstaloyCrM+x%C (x…0.6-1.4), presintered and then induction sintered, 400 K/min - 5 min - 600 K/min, 800 mbar N_2, 1370°C.

As can be clearly seen, the samples with 0.6-0.9 $\%C_{admixed}$ could be sintered to products with stable shapes. For the ones with higher carbon contents the temperature was definitely too high, too much liquid phase was formed, with adverse effect on shape retention. At this temperature, satisfactory SSPLS could be achieved for 0.9%C, as indicated by high shrinkage and metallic finish without losing shape.

Based on these first sintering results, the samples containing 0.6, 0.7, 0.8, $0.9\%C_{admixed}$ were sintered at higher temperatures (within 30°C steps), and the other samples with 1.0, 1.1, 1.2 and 1.4%C at lower temperatures, also in 30°C steps. In Table 2 the sample matrix for sintering at different temperatures is listed. In green, the applied induction sintering temperatures (until loss of shape takes place) for the respective carbon contents are highlighted.

Tab.2. Sample matrix, applied induction sintering temperature [°C] for AstaloyCrM+x$\%C_{admixed}$ (x…0.6-1.4)

C-content [wt%]	Temperature [°C]				
	1310	1340	1370	1400	1430
0.6					
0.7					
0.8					
0.9					
1.0					
1.1					
1.2					
1.4					

For all compositions a suitable induction sintering temperature, with high shrinkage and densification and retention of the shape at the same time, could be defined. For a better overview the determined sintered density (ρ_{sinter} in g/cm³) is plotted against the sintering temperature for the compositions AstaloyCrM+0.6, 1.0 and 1.4%C; see Figure 3.

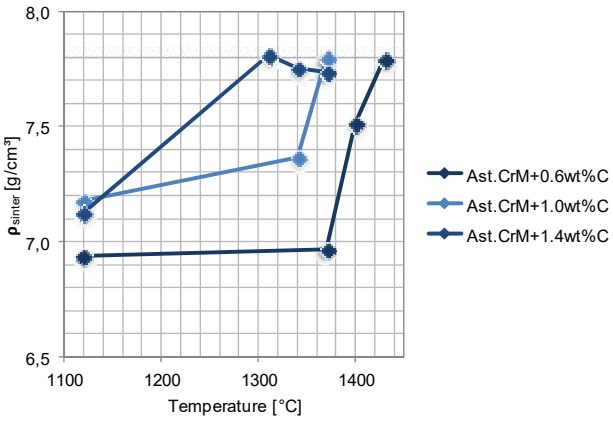

Fig.3. Sintered density vs. sintering temperature of AstaloyCrM+0.6, 1.0 and 1.4wt%C; after induction sintering, 400 K/min – 5 min - 600 K/min, 800 mbar N_2, at different temperatures.

The theoretical (pore-free) density is marked in light blue in the graphic; it is shown that all specimens with different compositions can be sintered to almost full density if the correct temperature is chosen. For 0.6 %C, even at a sintering temperature of 1370°C in the induction furnace hardly any densification occurs; the SSPLS process starts at markedly higher temperatures (1400°C). For AstaloyCrM+1.4%C, on the other hand, a sintered density of 7.8 g/cm³ can be attained already at 1310°C, while above this temperature oversintering occurs which results either in swelling of the sample or, at still higher temperatures, in complete melting.

In Figure 4 the unetched cross sections of the AstaloyCrM samples with the lowest carbon content (0.6%$C_{admixed}$) after all sintering steps are displayed (magnification 50x). In the specimen (a), induction sintered at 1370°C, considerable porosity can be detected, while after sintering at 1400°C, only a few small isolated pores can be found (b), i.e. SPLS is effective at this temperature. After sintering at 1430°C (c) huge pores were found sporadically distributed within the entire component. Explanations for that are on one hand too much liquid phase, and on the other hand a densification that has started in the surface zone before the gaseous products of carbothermal oxide reduction were removed, which results in these gas outbursts and in stabilizing large pores which act as sinks for the pore space from smaller pores, following the Ostwald ripening mechanism.

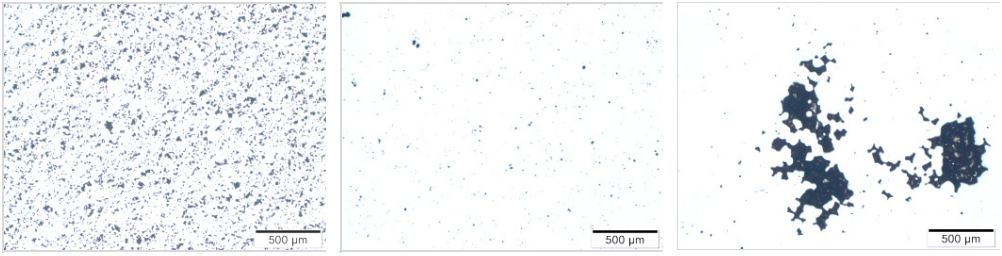

a) 1370°C b) 1400°C c) 1430°C

Fig.4. AstaloyCrM+0.6%C induction sintered at different temperatures, 400 K/min -5 min - 600 K/min, 800 mbar N2, 50x.

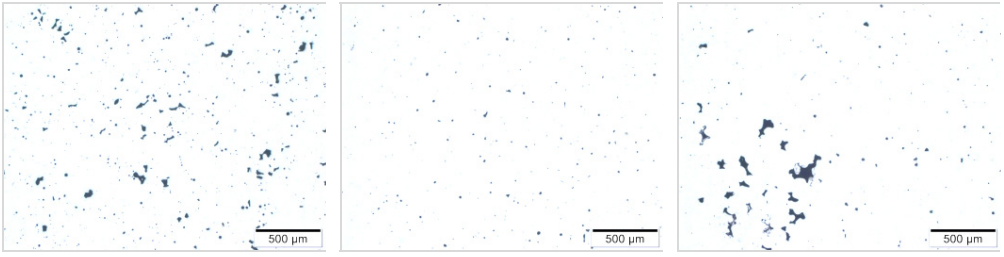

a) 1310°C b) 1340°C c) 1370°C

Fig.5. AstaloyCrM+1.4%C, induction sintered at different temperatures, 400 K/min - 5 min - 600 K/min, 800 mbar N_2, 50x.

In Figure 5 the polished cross sections of the sintered AstaloyCrM pieces with the highest carbon content (1.4%$C_{admixed}$) are shown as examples. After induction sintering at 1310°C an increase of density can be observed compared to e.g. Figure 4a, but also grain growth, this was already shown by the results of the previous study. The microstructure of the sample sintered at 1340°C (c) looks better/denser, but this piece could not be sintered

without losing its shape, and the same holds for 1370°C, because of oversintering. Also here, coarse pores appear, although not as massively as shown in Figure 4c; probably the lower temperature results in less pronounced reduction of stable oxides.

In Figure 6 and Figure 7 Nital etched microstructures are shown, again exemplary for the two compositions AstaloyCrM+0.6 and 1.4%C (magnification 200x).

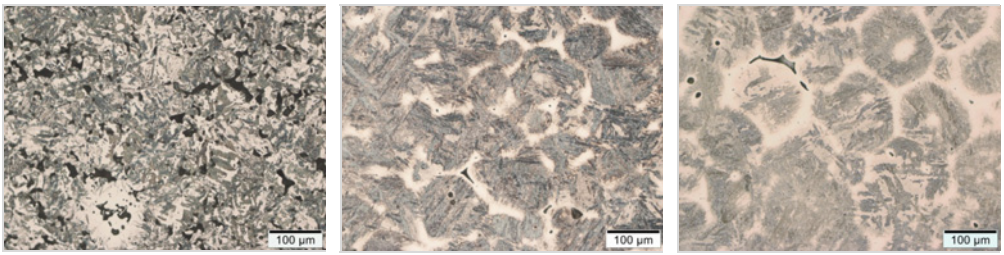

a) 1370°C b) 1400°C c) 1430°C

Fig.6. AstaloyCrM+0.6%C induction sintered at different temperatures, 400 K/min - 5 min - 600 K/min, 800 mbar N_2, 50x, Nital etched.

After induction sintering, bainitic microstructure is found due to the slower cooling rate of the furnace at lower temperatures whereby bainite can be stabilized. Coinciding with pronounced densification, strong grain growth can be observed as well. For grain refinement a subsequent heat treatment, similar to normalizing of cast steel components, would be useful.

For AstaloyCrM+1.4%C, induction sintering results in a clearly visible network of proeutectoid cementite formed at the grain boundaries during SSPLS; the same had been discovered after the preliminary sintering in the dilatometer (see above).

Furthermore, grain growth could be detected for this composition, already starting at 1310°C (Fig.7a) because of the decrease of porosity which normally prevents grain growth [13]. Deceptively, the specimens of the composition AstaloyCrM+1.4%C induction sintered at 1340 (c) and 1370°C (d) seem to have quite attractive densities, however both samples were totally oversintered and had lost their shape. The same trends were observed for all other compositions, just the temperature level for optimum sintering varying with carbon content.

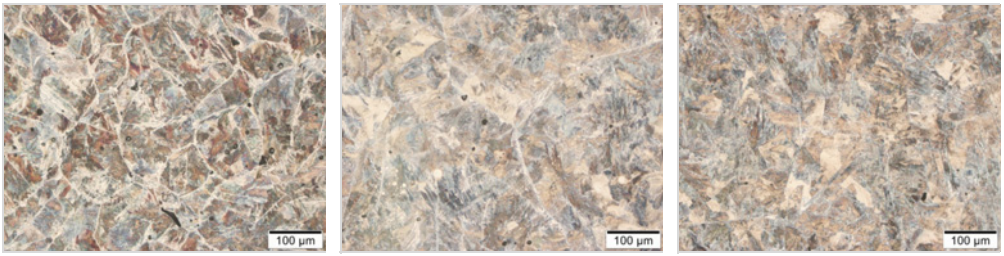

a) 1310°C b) 1340°C c) 1370°C

Fig.7. AstaloyCrM+1.4%C induction sintered at different temperatures, 400 K/min - 5 min - 600 K/min, 800 mbar N_2, 50x, Nital etched.

For further analysis the macrohardness (HV30) of all samples was measured to observe densification effects and consequently the increase of hardness. As representative

examples the results of the samples AstaloyCrM+0.6, 1.0 and 1.4%C are depicted in the following histograms (Figure 8).

Analysis of the hardness trends induces the conclusion that the process of densification due to supersolidus liquid phase sintering can be described quite well by hardness measurements, but no statements concerning oversintering can be produced.

The HV30 values of AstaloyCrM+1.4%C show quite well that a temperature above 1310°C does not lead to higher densities, already the material sintered with 1310°C has hardly any porosity left. At the same time no hardness loss was measured although the samples lost their shape at higher temperatures. The same applies for Ast.CrM+1.0%, in which case the highest density could be obtained after induction sintering at 1370°C, but this sample was not sintered dimensionally stable. As shown in Fig.8 and confirmed by micrographs, the presintered AstaloyCrM-0.6wt%C sample has quite a high hardness (because of existing martensitic structures). After sintering at 1370°C a drop of hardness could be noticed because of the "low" cooling rate, but at 1400°C, as SSLPS occurred, an increase of hardness was recorded again. In this case the oversintering of the sample could be detected; the material sintered at 1430°C shows a low hardness value again.

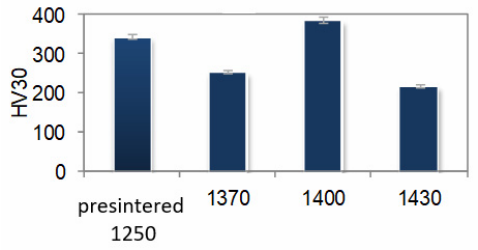

a) AstaloyCrM+0.6wt%C

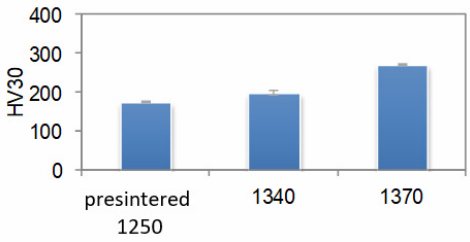

b) AstaloyCrM+1.0wt%C

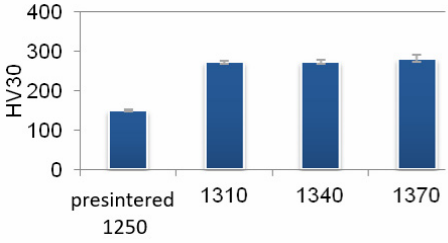

c) AstaloyCrM+1.4wt%C

Fig. 8. Hardness HV30 of AstaloyCrM-samples, induction sintering, 400 K/min - 5 min - 600 K/min, 800 mbar N_2; as a reference, hardness from presintered samples (1250°C) is given.

CONCLUSIONS

The preliminary sintering experiment done in a dilatometer on Cr-Mo prealloyed AstaloyCrM with a quite high carbon content of 1.0% showed that high densification by SSPLS can be also attained with chromium containing low alloy steels. On the negative side, grain coarsening and a network of proeutectoid cementite could be observed as well.

Further investigations have been performed with induction sintering, which enables attaining the high temperatures necessary for SSLPS more easily. Sintering was done in a two-step-process, first conventional solid state sintering in a pusher furnace and then induction SSLPS for a short time. This was applied for a carbon content that was

varied from 0.6 to 1.4%, whereby supersolidus liquid phase sintering occurred for all compositions, though at different temperatures. A suitable induction sintering temperature, resulting in high shrinkage and shape retention at the same time, could be found for all compositions, though at different levels. Micrographs (polished and etched) showed that above a critical temperature huge pores were found that are statistically distributed over the entire component, due to concurrent densification and formation of gas products, which results in gas outbursts and damage to the specimens. Grain growth was detected for all compositions, starting at temperatures where pronounced densification through SSPLS occurs, because of the dramatic decrease of porosity which normally prevents grain coarsening very effectively in sintered steels. For higher carbon contents a network of proeutectoid cementite was formed at the grain boundaries during SSPLS; similar to that observed after sintering in the dilatometer. For both problems, grain coarsening and proeutectoid cementite, a suitable heat treatment would be the remedy, as known e.g. from casting of steels.

In general it can be stated that supersolidus liquid phase sintering can be applied for chromium steels, leading to almost full density while the specimen shape is retained. Both conventional and induction heating can be applied, the latter being an attractive solution for steels with lower C levels that require very high sintering temperatures. The most important items are selecting and maintaining the optimum sintering temperature for the given carbon level. Furthermore, attaining oxygen removal by a solid state sintering process before the densifying induction process was found to eliminate the formation of gas pores and blisters if induction sintering was done in the proper temperature interval.

REFERENCES

[1] German, RM.: Sintering Theory and Practice. New York : John Wiley & Sons, Inc., 1996
[2] Huemer, M., Gierl-Mayer, C., Danninger, H. In: PM2014 World Congress on Powder Metallurgy & Particulate Materials. Orlando, 2014
[3] Schatt, W.: Sintervorgänge. Düsseldorf : VDI Verlag, 1992
[4] German, RM.: Int. J. Powder Metall. & Powder Technol., vol. 19, 1983, no. 4, p. 277
[5] Gierl-Mayer, C., Danninger, H., De Oro, R., Hryha, E. In: Advances in Powder Metallurgy and Part. Materials 2014. Proceedings of World PM Orlando, Florida May 18-22 2015. Eds. RA. Chernenkoff, WB. James, p. 05-74
[6] Lund, JA., Bala, SR.: Powder Metall., vol. 6, 1974, p. 409
[7] German, RM.: Int. J. Powder Met., vol. 26, 1990, p. 23
[8] Liu, J., Upadhyaya, A., German, RM.: Metallurg. & Mat. Trans. A, vol. 30A, 1999, no. 8, p. 2209
[9] Danninger, H., Gierl, C.: Materials Chemistry and Physics, vol. 67, 2001, no. 1-3, p. 49
[10] Liu, J., Lal, A., German, RM.: Acta Mat., vol. 47, 1999, no. 18, p. 4615
[11] Huppmann, WJ.: Int. J. Powder Metall. & Powder Technol., vol. 21, 1985, no. 3, p. 183
[12] Gierl-Mayer, C.: Herstellung von hochdichten PM-Präzisionsteilen durch optimierte Sinterverfahren. Ph.D Thesis. Wien : TU, 2000
[13] Mohammadzadeh, A., Azadbeh, M., Danninger, H.: Powder Metallurgy, vol. 58, 2015, no. 2, p. 123
[14] Schatt, W., Wieters, K-P., Kieback, B.: Pulvermetallurgie – Technologien und Werkstoffe, 2., bearbeitet Auflage. Berlin, Heidelberg, New York : Springer Verlag, 2007
[15] Upadhyaya, A., Upadhyaya, GS.: Powder Metallurgy – Science, Technology and Materials. Hyderabad, India : Universities Press, 2011

[16] Hermel, W., Leitner, G., Krumphold, R.: Powder Metallurgy, vol. 23, 1980, no. 3, p. 130
[17] Šalak, A.: Ferrous Powder Metallurgy. Cambridge : International Science Publishing, 1997
[18] Dlapka, M., Strobl, S., Danninger, H., Gierl, C.: Practical Metallography, vol. 47, 2010, no. 12, p. 686

sciendo
Powder Metallurgy Progress, Vol.19 (2019), No.2, p.063-081
http://dx.doi.org/10.1515/pmp-2019-0007

ADDITIVE MANUFACTURING OF STEEL AND COPPER USING FUSED LAYER MODELLING: MATERIAL AND PROCESS DEVELOPMENT

J. V. Ecker, K. Dobrezberger, J. Gonzalez-Gutierrez, M Spoerk, Ch. Gierl-Mayer, H. Danninger

Abstract

Fused Layer Modelling (FLM) is one out of several material extrusion (ME) additive manufacturing (AM) methods. FLM usually deals with processing of polymeric materials but can also be used to process metal-filled polymeric systems to produce metallic parts. Using FLM for this purpose helps to save costs since the FLM hardware is cheap compared to e.g. direct metal laser processing hardware, and FLM offers an alternative route to the production of metallic components.

To produce metallic parts by FLM, the methodology is different from direct metal processing technologies, and several processing steps are required: First, filaments consisting of a special polymer-metal composition are produced. The filament is then transformed into shaped parts by using FLM process technology. Subsequently the polymeric binder is removed (''debinding'') and finally the metallic powder body is sintered. Depending on the metal powder used, the binder composition, the FLM production parameters and also the debinding and sintering processes must be carefully adapted and optimized.

The focal points of this study are as following:

1. To confirm that metallic parts can be produced by using FLM plus debinding and sintering as an alternative route to direct metal additive manufacturing.

2. Determination of process parameters, depending on the used metal powders (steel and copper) and optimization of each process step.

3. Comparison of the production paths for the different metal powders and their debinding and sintering behavior as well as the final properties of the produced parts.

The results showed that both materials were printable after adjusting the FLM parameters, metallic parts being produced for both metal powder systems. The production method and the sintering process worked out well for both powders. However there are specific challenges in the sintering process that have to be overcome to produce high quality metal parts. This study serves as a fundamental basis for understanding when it comes to the processing of steel and copper powder into metallic parts using FLM processing technology.

Keywords: additive manufacturing, 316L stainless steel powder, Cu powder, properties, mcrostructure

Josef Valentin Ecker, Klaus Dobrezberger, Christian Gierl-Mayer, Herbert Danninger: Technische Universität Wien, Getreidemarkt 9/164, 1060 Wien, Austria

Joamin Gonzalez-Gutierrez, Martin Spoerk: Polymer Processing, Montanuniversitaet Leoben, Otto Gloeckel-Strasse 2, 8700 Leoben, Austria

INTRODUCTION

The most common type of material extrusion additive manufacturing (MEAM) is a low-cost process in which a filament is softened, and the soft material is pushed through an orifice, The extrudate is then selectively deposited layer-by-layer to shape a three-dimensional object [1]. It has been demonstrated that it is possible to use MEAM for the production of complex-shaped parts not only made out of thermoplastics [1–14] and low melting point metals alloys, but also high-melting-point metallic alloys [1, 15–19], ceramics [20–33], and cermets [34]. In order to obtain metallic, ceramic and cermet parts, highly-filled filaments are used as the feedstock material; the shaped part is then subjected to a process of binder removal and sintering to densify the parts [1], similar to the procedure common in powder injection moulding [2].

Copper parts can be additively manufactured by several methods such as powder bed fusion and binder jetting [35]. Parts obtained by powder bed fusion using electron beam melting tend to have defects caused by the severe dissipation of thermal energy during the melting process, as a consequence of the high thermal conductivity of copper. When using laser-based melting techniques, with copper powders densities of up to 99.9% can be obtained; however higher power is required (1000 W) compared to steels (200 W), due to the lower absorption of the laser radiation and the higher thermal conductivity of copper, which further increases the cost of the AM equipment.

In this investigation we concentrate on the production of steel and copper parts by MEAM.

Additive manufacturing (AM) in general has emerged as a technology for manufacturing parts with complex geometrical features that are not easily obtainable by conventional shaping or subtractive techniques [1]. AM holds the potential to make manufacturing processes more sustainable by improving resource efficiency, extending product life by easy repair, and simplifying supply chains [3–7]. There are numerous variants of AM [8]. For metal parts, powder bed fusion systems and direct energy deposition processes [8] (selective laser melting – SLM, electron beam melting – EBM, and laser-engineered net shaping – LENS) are the preferred methods for manufacturing such complex parts in short production runs [1, 10]. However, it has been shown that other AM techniques can be used to shape metal parts indirectly [10], namely binder jetting [12] and material extrusion (ME) [8]. Especially ME, also known as fused filament fabrication (FFF) [13–15], fused deposition modeling (FDM^{TM}) [16–18], or fused layer modeling (FLM) [19], henceforth always referred to as FLM, is of considerable interest, since it is the only AM technique that offers a manageable processability of an extensive variety of highly-filled materials [8, 20–24]. In FLM, a material in semi-liquid state (solid powder in a viscous matrix) is selectively deposited through an orifice according to a pre-defined computer aided design (CAD) model. The material passes through a nozzle, and the printing head or the building platform moves in x-y plane in order to form a layer of a part. After the completion of one layer, the printing head moves up or the building platform moves down (along the z-axis) so that the next layer can be deposited on top of the previous one [11]. Next to plunger- and screw-based printing heads, the filament-based design is by far the most popular one, due to the inexpensive acquisition costs and the ease of use of the machines [8].

The most common way to use FLM for metal part production is to follow the process known as Shaping, Debinding, and Sintering (SDS, Fig.) [25, 26]. Therefore, a highly-filled compound consisting of a thermoplastic binder and metallic powder needs to be prepared. After extruding this compound to filaments, parts of complex shape are

formed by inexpensive FLM machines. Subsequently, these parts are debinded, in which stage the polymeric binder is partially removed from the shaped part without damaging the printed specimen, either by using solvents and/or by thermal degradation, only a minor binder component – the "backbone" - remaining. Finally, the debinded part is placed in a conventional sintering furnace to remove the last binder components, coalesce the metallic particles and densify the shaped specimen. The SDS process has been used for decades in metal injection molding (MIM) [2] and since the 1990's with FLM machines [27, 28, 29].

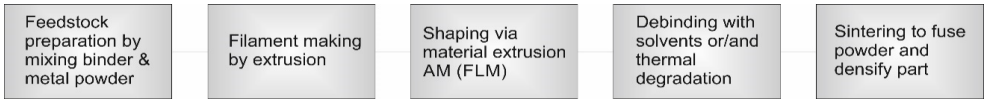

Fig.1. Flow chart of the shaping, debinding and sintering (SDS) process.

One of the main limitations to use filament-based FLM is that most commercially available highly-filled polymers used in MIM do not meet all the property requirements to be processable in conventional filament-based FLM machines. Binder modifications are necessary because MIM feedstocks are designed for good flowability so that the cavity of the injection molding tool can be filled completely at moderate pressures. On the other hand, FLM feedstocks need to have enough stiffness, strength and flexibility so that the filaments can be processed in the FLM machine and that the filaments can be wound in a spool for continuous material feeding. A comparison between the binders used in MIM and in FLM is shown in a literature review [8].

In previous investigations it has been demonstrated that the SDS process can be done with a variety of metal or ceramic materials, using different binder and feedstock compositions [8]. However, it has not been directly investigated how changing the chemical composition and particle size distribution of fillers affects the FLM process of highly-filled filaments. In this paper, we demonstrate that by using one binder system, different metallic systems can be shaped in a simple and inexpensive FLM machine. The selected metals comprise stainless steel and copper, which are metallic materials with different densities and chemical compositions used in numerous industrial applications. Here, the effect of the different fillers on the first three stages of the SDS process was investigated, namely: (i) the feedstock preparation, (ii) the filament making process, and (iii) the shaping by FLM. The properties of the feedstocks and filaments that affect the processability by FLM are also presented. Therefore, the apparent viscosity is presented to compare the flow behavior of feedstocks with the different fillers. Moreover, the mechanical and morphological characteristics of the different filaments are presented and discussed. This paper aims to provide some insight into what the important material properties and processing parameters are that are needed to produce parts by FLM with different highly filled systems.

MATERIALS

A combination of a thermoplastic elastomer (Kraiburg TPE GmbH & Co. KG, Germany) and a grafted polyolefin (BYK-Chemie GmbH, Germany) was used as the binder system. The exact formulation of the binder system developed at the Montanuniversitaet Leoben is considered a trade secret and therefore will remain confidential. Two types of metallic powders were investigated: 316L stainless steel powder (Epson Atmix Corporation, Japan) and 99.9% pure copper powder (Cu 99.9, Carpenter Powders Products Inc., RI, USA). All powders were gas atomized and are therefore spherical-shaped (Chyba! Nenalezen zdroj odkazů.). The particle size data as supplied by the producers are shown in

Tab.. It can be seen that stainless steel has the smallest particles, though with wide size distribution, while copper shows also larger particles.

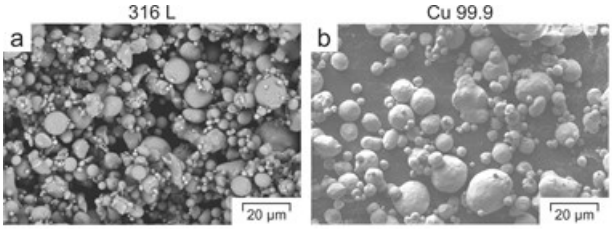

Fig.2. Scanning electron microscopy (SEM) images of the investigated powders 316 L (a) and Cu 99.9 (b).

Tab.1. Particle size data for metal powders used in feedstocks.

Percentile ranks	**316 L**	**Cu 99.9**
D_{10} (µm)	3.49	5.04
D_{50} (µm)	5.53	14.55
D_{90} (µm)	8.47	29.69

METHODS

Preparation of feedstocks for processing via Fused Layer Modelling

Binder preparation

The binder was prepared by pre-mixing the pellets of the thermoplastic elastomer with those of the grafted polyolefin in solid state. This pre-mixture was then extruded in a single screw extruder (FT-E20T-MP-IS, Dr. Collin GmbH, Germany) equipped with a round die of 1.75 mm in diameter. The extruded binder was cooled down in a water bath and later granulated in a strand pelletizer (SGS 50-EL, Scheer Reduction Engineering GmbH, Germany). The rotational speed of the screw was set to 70 rpm, the temperature profile in the barrel to 180, 195, and 200 °C, and the die temperature to 200 °C.

Feedstock compounding

All feedstocks were prepared with a constant powder content of 55 vol% in a co-rotating twin-screw extruder (ZSE 18 HP-48D, Leistritz Extrusionstechnik GmbH, Germany) with two gravimetric feeding units (DDW-M-DSR28, Brabender Technologie GmbH, Germany). The binder was placed in the first feeding unit, and the metal powder in the second one. The rotational speed of the screw was set to 600 rpm, and the temperatures from the feeding zone to the die were 25, 180, 180, 190, 200, and 210 °C. The temperature profile was established by six temperature-controlled heating bands installed along the extruder. The extrudate was transported on an air-cooled conveyor belt (Reduction Engineering Scheer, OH, USA) and pelletized in the strand pelletizer described above. Henceforth, all feedstocks are abbreviated by F-powder, e.g. F-316L for the feedstock filled with the 316 L stainless steel powder.

Filament production

Filaments were produced in the same single screw extruder in which the binder was prepared, equipped with a round die of 1.75 mm in diameter and 20 mm in length. However, the extrudate was not water cooled but cooled down by natural convection during the transportation on a conveyor belt (GAL-25, Geppert-Band GmbH, Austria) and a haul-off unit (self-developed). After the haul-off unit, the extruded filament's diameter and ovality was controlled to be 1.75 ± 0.05 mm and <0.1 mm, respectively, by a diameter measurement device and a processor (Sikora Laser 2010T and EcoControl 600, Sikora AG, Germany), and the filaments were stored in spools. The extrusion temperatures and rotational speed were adjusted for each of the feedstocks (Tab.) to accommodate for the different thermal conductivity, flow properties, and mechanical properties of the different feedstock materials. Apart from minor differences in the temperatures, the biggest difference was observed in the rotational speed of the extrusion screw. If the extrudate has enough melt strength and the solid filament has enough tensile strength, the filament can be extruded at a faster rate.

Tab.2. Extrusion parameters for the filament preparation of the two feedstocks investigated.

Extrusion parameters	**F-316L**	**F-Cu99.9**
Temperature of the feeding zone (°C)	180	180
Temperature of the compression zone (°C)	190	190
Temperature of the metering zone (°C)	200	195
Temperature of the die (°C)	200	200
Screw rotational speed (rpm)	39	85

Fused Deposition Modeling – production of samples

Printing trials were performed on an FLM printer X1000 (German RepRap GmbH, Germany), on which the printing head was completely replaced by a self-made dual drive extruder system. For establishing the printing parameters, thin-walled cylinders, each having a wall thickness of 1.3 mm, height of 48 mm, outer diameter of 32 mm, were printed as shown in Fig.2. Subsequently, also other shapes were produced (see below, Chapter 3).

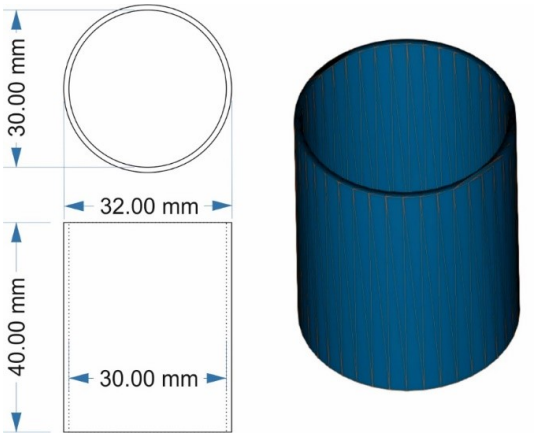

Fig.3. CAD drawing of thin walled cylinders produced by FLM.

For the F-Cu 99.9 filament, it was necessary to increase the extrusion temperature to 240 °C, as problems with buckling of the filament occurred at 235°C during printing. The problem vanished when printing at 240°C due to a reduction of the viscosity of the molten feedstock.

Tab.3. Printing parameters used for the different shaped test samples (cylinders, plates, porous cylinders).

Printing parameters	**F-316L**	**F-Cu99.9**
Nozzle diameter (mm)	0.6	0.6
Layer height (mm)	0.24	0.30
Printing speed (mm/s)	50	30
Extrusion temperature (°C)	235	240
Platform temperature (°C)	90	90
Platform material	Glass	Glass
Infill (%)	100	100

Solvent debinding

During the debinding process, the organic binder (polymer) is largely removed by dissolving it, only the backbone component remaining. Cyclohexane is used as a solvent at its boiling temperature (81°C) to secure a constant temperature. The solvent was stirred by means of a magnetic stirrer, whereby the component was placed on a wire mesh to exclusively stir the solvent. The beaker was covered with a watch glass. (Fig.). In order to guarantee successful further sintering steps, debinding using a suitable solvent is essential. Care must be taken to ensure gentle conditions (solvent, temperature) [36]. Drying was carried out in room air at room temperature for several hours, normally overnight.

Fig.4. Beaker filled with cyclohexane for debinding.

Thermal debinding and sintering

Remaining organic binder residues – the backbone component that ensures sufficient strength of the solvent debinded part - are removed by thermal debinding after the solvent removal process, typically in the early stages of the sintering process, i.e. during heating. Subsequently, sintering takes place, whereby the powder particles form solid metallic bridges, the porosity is reduced and consequently the component shrinks. This results in a solid metallic shape. Sintering requires temperatures of at least around 1000°C and has been done in an electrically heated tube furnace (pusher furnace with steel muffle, 1.4841). For 316L, sintering was performed at 1350°C in a Nabertherm furnace with Al_2O_3 muffle in dry hydrogen (Air Liquide, Alphagaz, 99.999). Hydrogen humidified by bubbler was used for the sintering of copper. The bubbler was filled with water at room temperature. Sintering processes of various materials have also been thoroughly investigated by Danninger et al. [37–40].

Dilatometry

Dilatometric measurements were performed using a Netzsch 402C pushrod dilatometer with Al_2O_3 measuring system. Those measurements are very important for the determination of dimensional changes as described in [41]. Only Cu samples were examined in the dilatometer to find the cause of the deformation described below. Dry hydrogen was used as atmosphere.

Mass spectrometry

Mass spectrometry measurements were carried out using a Netzsch Aeolos QMS 403C with capillary coupling to the dilatometer.

Density measurement and porosity

The density was measured using the Archimedes principle, where a Mettler Toledo density scale was used. The porosity was calculated from the measured and theoretical density values. Density measurements and porosity are very important techniques to characterise the various properties of sintered materials. [42, 43].

Microscopy of sintered samples

Microscopic examinations were performed using a Zeiss Observer D1 optical microscope. Fine structures of the material can only be determined by microscopic (light and/or electron microscopy) methods. V2A etching agents for steel and Heyn etching agents for Cu (copper ammonium chloride in H_2O) were used as etching agents, and the microstructures were then examined by light microscopy [43, 44].

Determination of carbon and oxygen content

The carbon content was measured using a LECO CS230 combustion analyzer, and the measurement of the oxygen content was performed by inert gas fusion with a LECO TC 400. The analysis of carbon and oxygen is a very important task since esp. carbon influences the sintering process. The behavior of carbon on sintering of nonferrous metals such as Cu and Al has been the subject of work in the past [45, 46]. For stainless steels the carbon content should be below 0.02% to prevent intergranular corrosion.

RESULTS AND DISCUSSION

Stainless steel samples

Samples and specific printing parameters

The samples E1 and E2 are tubes with approx. 48 mm height & 32 mm outer diameter and 1.3 mm wall thickness. In contrast, the samples E3 to E5 are plates with a structured surface, approx. 30 x 30 mm² and 1.25 mm thickness. All specimens were produced by the FLM method.

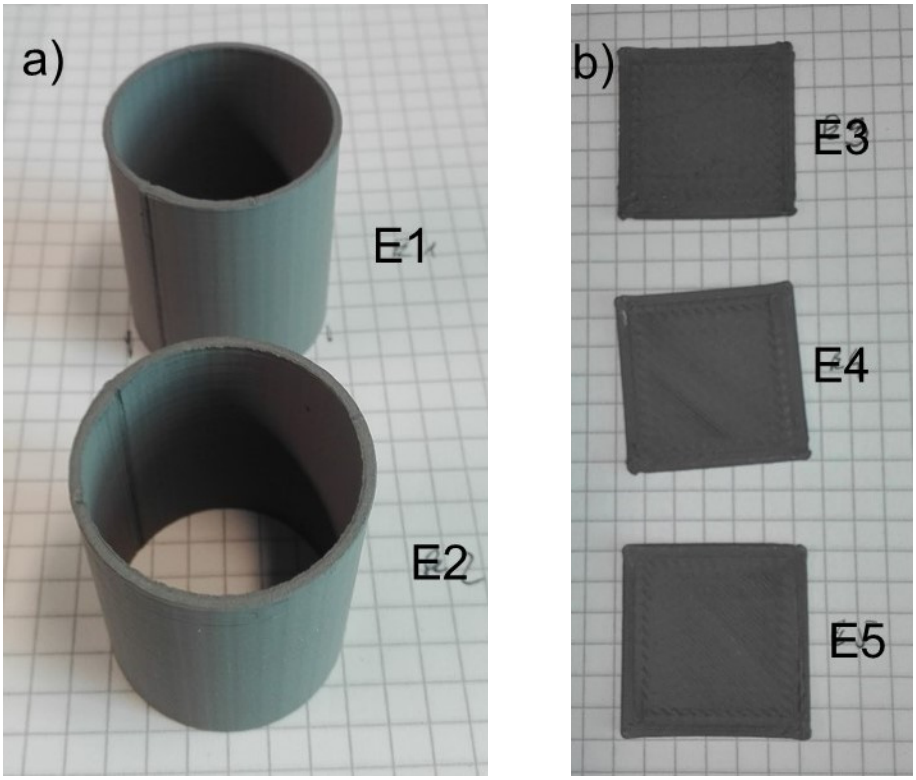

Fig.5. Untreated (as printed) samples E1, E2 (a) and E3, E4 and E5 (b).

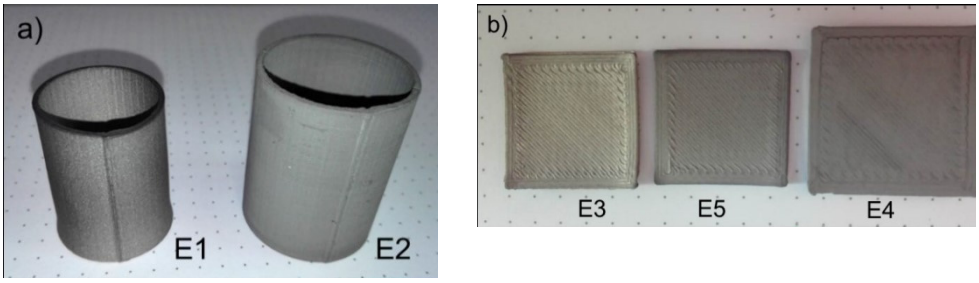

Fig.6. Samples E1 (sintered) and E2 (debinded) (a) and E3 (sintered), E5 (sintered) and E4 (debinded).

Samples E1, E3 and E5 were used for experiments regarding sintering. E2 and E4 were just debinded with cyclohexane.

Debinding

Solvent debinding was carried out as described above with magnetic stirring using. cyclohexane. Weight loss was determined by weighing the sample before and after solvent debinding with cyclohexane; data are shown in Tab.. Drying was again carried out in room air at room temperature overnight.

Tab.4. Mass loss during solvent debinding of stainless steel specimens.

Sample name	Mass loss [%]
E1	5.63
E2	5.65
E3	5.81
E4	5.72
E5	5.85

Sintering

The sintering temperature was 1350°C, and a heating rate of 5 K/min was set to heat up to this temperature. It was then kept isothermal for 60 minutes. The samples E1, E3 and E5 were sintered. As stated above the atmosphere was high purity hydrogen.

Density, porosity and C content

E1 has a relatively low porosity compared to E5. The carbon content was determined in samples E1 and E3 and is very low, which indicates that thermal debinding has been done correctly. The results are shown in Tab.. There are some differences in porosity; However, this parameter is difficult to quantify in the specimen section due to the coarse porosity in the gussets, which at least in laboratory tests may vary slightly between the printing jobs although the conditions for printing the specimens were set identical. The dimensional change of the specimens during sintering could be estimated. For the plate sample E5, the dimensional change is -15.8 % (dimensions from 30 mm to 25.25 mm). With the cylindrical sample E1, the radial change of the outer diameter is -15.3 % (dimensions of the outer diameter changed from 31.52 mm to 25.86 mm). The dimensional change during sintering is therefore comparable and similar between the components.

Tab.5. Density, porosity and C content of stainless steel specimens.

Sample	Density [g/cm^3]	Porosity [%]	C Content [µg/g]
E1	7.39	7.64	97 ± 9
E3	7.44	6.95	107 ± 11
E5	7.24	9.49	not determined

Microstructure

Microscopic examination of unetched and etched samples was performed at different magnifications. V2A pickle was used as an etchant. The etched structure (Fig.) corresponds to austenitic stainless steel, whereby no carbides are recognizable, which in turn agrees with the very low C content indicated by LECO analysis.

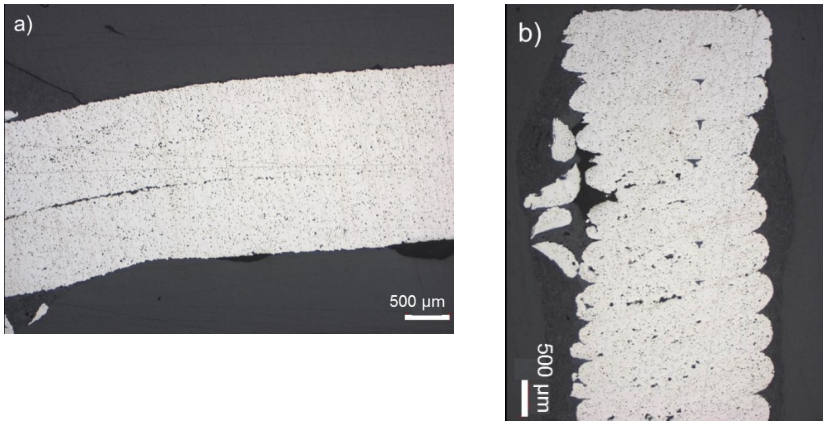

Fig.7. Unetched section of E1 with 50x, parallel (a) and transverse to direction of construction (b).

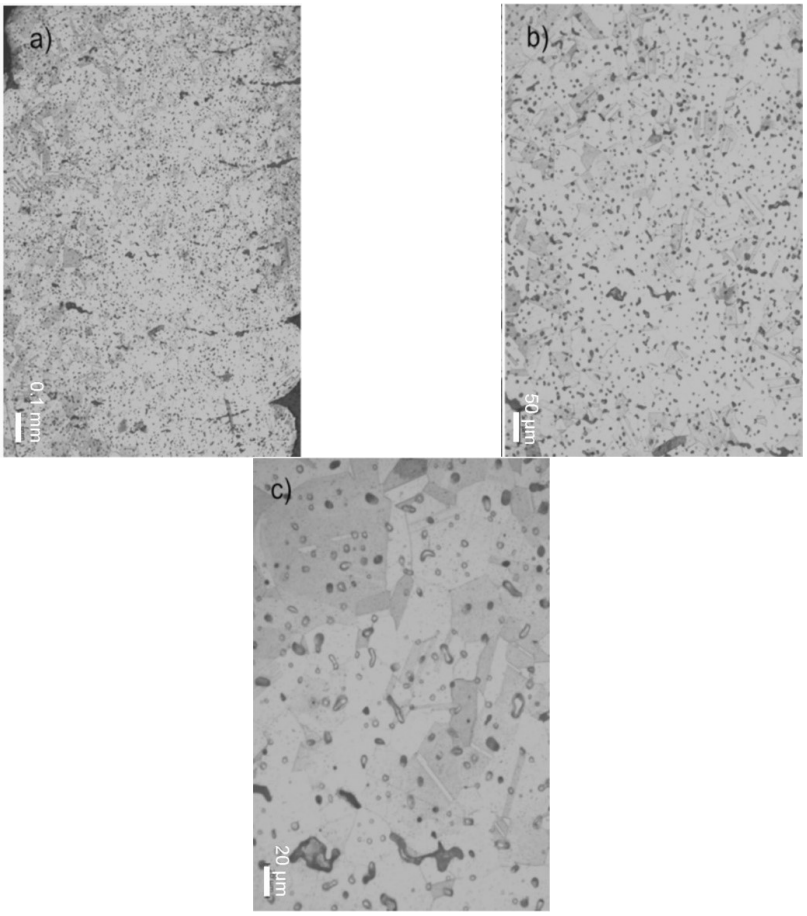

Fig.8. Etched section of sample E1 100x(a), 200x (b) and 500x (c) with grinding transverse to the direction of construction.

Microscopy shows two types of porosity: fine, evenly distributed pores, which can hardly be avoided in solid state sintering, estimated at approx. 2%, and large pores from the gussets of the printing process, which cannot be reduced or eliminated by sintering and must be avoided during printing. The etched structure conforms to austenitic stainless steel. Once more there are no carbides visible (which are not to be expected at the measured C content).

Cu-sample

Samples and specific printing parameters

Samples of different shapes were prepared by FLM printing. The samples are shown below with their designations.

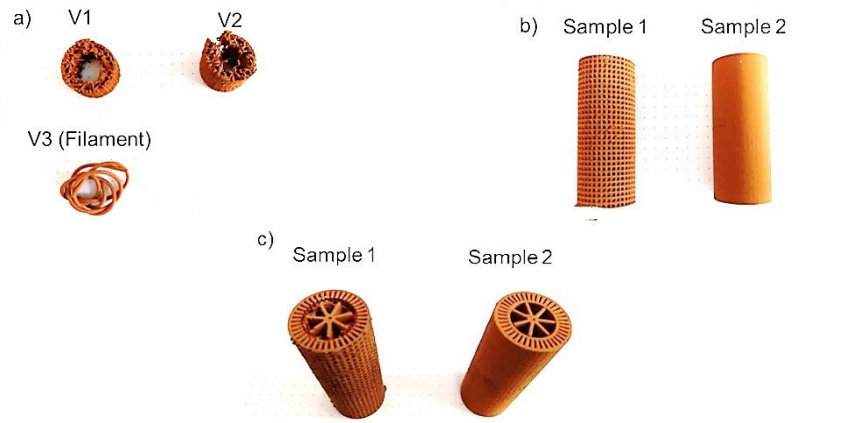

Fig.9. Original samples before debinding. V1, V2 and V3 (a), Sample 1, Sample 2 (b) and Sample 1, Sample 2 on top (c)

Debinding

The procedure of debinding was the same as with the steel samples. Mass loss was determined by weighing the sample before and after treatment with cyclohexane and drying in room air at room temperature overnight. Sample V2 was completely unfolded/deformed after the debinding procedure (Fig. a). The mass loss data are shown in the following (Tab.).

Tab.6. Mass loss of different printed Cu based samples during solvent debinding

Sample name	Mass loss [%]
V1	5.29
V2	5.33
V3 (filament)	5.14
Sample 1	5.03
Sample 2	4.79

It is obvious that the mass loss of all samples is in the range of about 5 % without significant differences between each other. Thus, the mass loss seems to be independent of the sample shape.

Sintering

Sintering of the samples was carried out in the pusher furnace with steel muffle in humid H_2 atmosphere, whereby the humidification was carried out with a bubbler at a dew point of 25°C. The heating rate was 5 K/min with a maximum temperature of 1060°C held for 60 minutes. The larger sample bodies (Sample 1 and Sample 2) were positioned horizontally in an alumina crucible and thus fed to the sintering process.

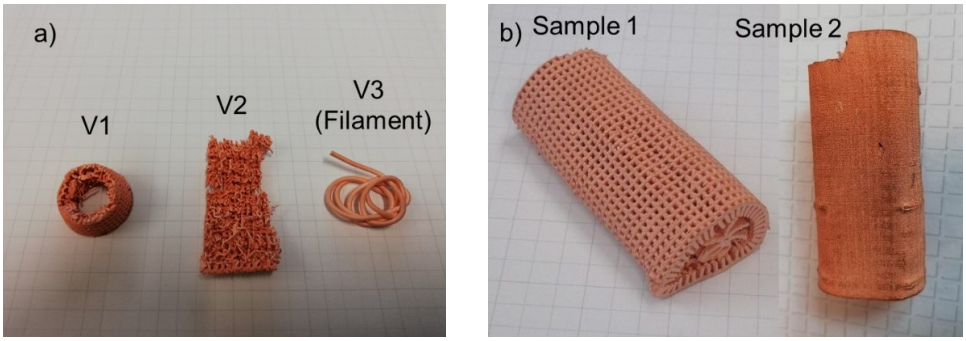

Fig.10. Samples after the sintering process. V1, V2 and V3 a) and Sample 1 and Sample 2 b).

Fig.11. Original sample for test series.

As can be seen, the small specimens V1-V3 more or less retained their shape after sintering, V1 exhibiting some conical distortion. The larger and much heavier specimens Sample 1 and 2, in contrast, were heavily deformed and partially collapsed under their own weight. This collapsing might have occurred during isothermal sintering; however it was also imaginable that melting of the remaining binder, the backbone, had occurred at a low temperature at which hardly any metallic contacts had been formed between the Cu particles, this melting having resulted in lubrication between these particles and thus in loss of structural rigidity.

In order to potentially overcome this latter problem, two series of tests were carried out during sintering. For this purpose, a 30 mm high sample similar to Sample 1 was used (Fig.) that had been solvent debinded as described above.

In test series 1, shock debinding was carried out, with the aim of preventing deformation of the sample in the range of 124°C, because PE in the backbone starts melting at this temperature. This was to be achieved by producing only gaseous binder burnout

products which do not lubricate and thus should not cause any deformation of the specimen, i.e. to avoid liquid binder at all. The test run was carried within a sintering process. For this purpose, the furnace was preheated to 400°C and the sample was introduced. After isothermal temperature control for 30 minutes, the furnace was then heated to 1050°C at 10 K/min. After the process, the inspection revealed that nevertheless some slight deformation of the components had occurred (Fig.).

In test series 2, an even more severe shock debinding was applied to enhance the effect. The furnace was preheated to 1050°C and the sample introduced.

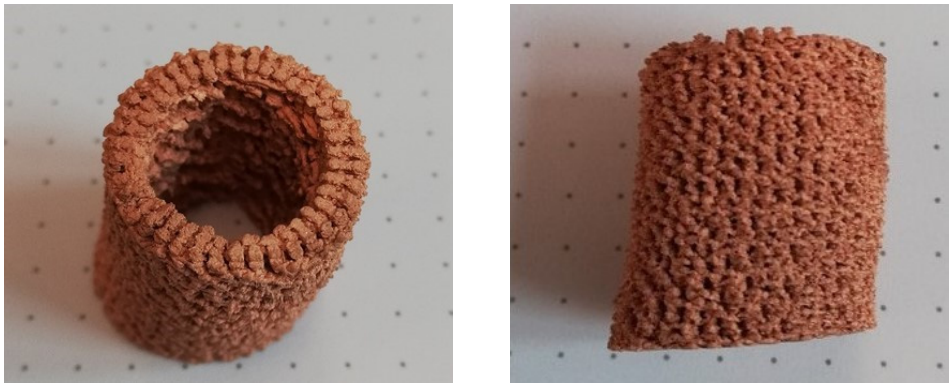

Fig.12. Sintered sample after test series 1.

Fig.13. Sintered sample after test series 2.

Dilatometry and mass spectrometry

Dilatometry tests were performed as follows: 8 mm thick samples were cut out of sample 2 (see Fig. b). The samples were solvent debinded, dried, placed into the pushrod dilatometer and heated at 5 K/min to a maximum temperature of 1030°C in flowing hydrogen atmosphere. The dilatometer was coupled with a mass spectrometer to detect any decomposition products of the binder. When the maximum temperature of 1030°C was reached, the temperature was maintained for 60 min (isothermal), and then the dilatometer was cooled down again to room temperature.

A strong shrinkage occurs at approx. 120°C, as shown in Fig.**,** because PE melts at this temperature. This can lead to a softening of the material at this temperature with resulting loss of strength. A water peak (m/z=18) appears at a temperature of 200°C, indicating the reduction of surface oxides. CO (m/z= 28), CO_2 (m/z= 44) and CH_4 (m/z=

16) are assumed from the detected masses at approximately 400°C, at which temperature sinter bridges can also be formed. However, atomic oxygen can also occur at m/z= 16 and N_2 at m/z= 28, which has the same molecular mass as CO, rendering parallel detection of O and CH_4 as well as N_2 and CO difficult. However, at 400°C it is evident that also a peak of m/z= 12 (carbon) and m/z= 15 is visible, which indicates a CH_3 fragment from methane and thus supports the theory that indicates the compounds CO, CO_2 and CH_4. Thus, it can be assumed that the residual binder is removed at this temperature (Fig.**).** Dilatometry shows further shrinkage at about 400°C, which is another indication of the removal of the organic binder and also for the adverse effects exerted on sintering of Cu by carbon containing compounds.

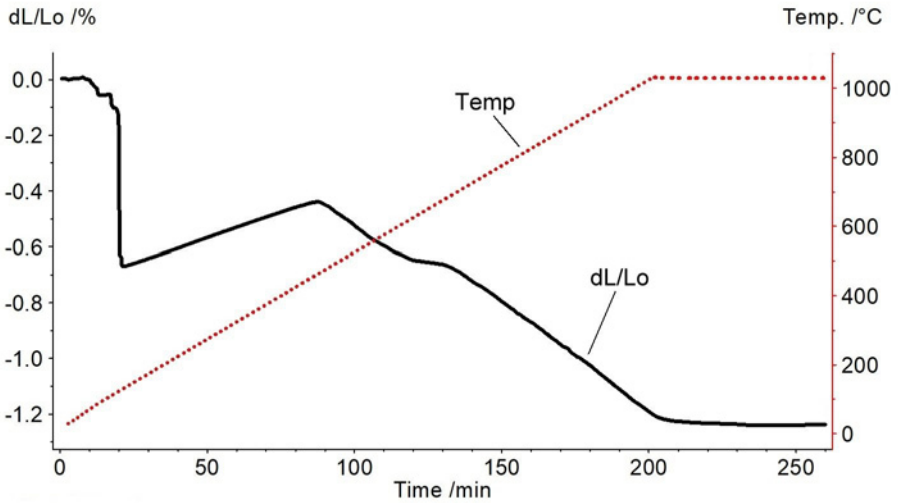

Fig.14. Dilatometry of Cu sample with a temperature ramp of 5 K/min and an isothermal temperature.

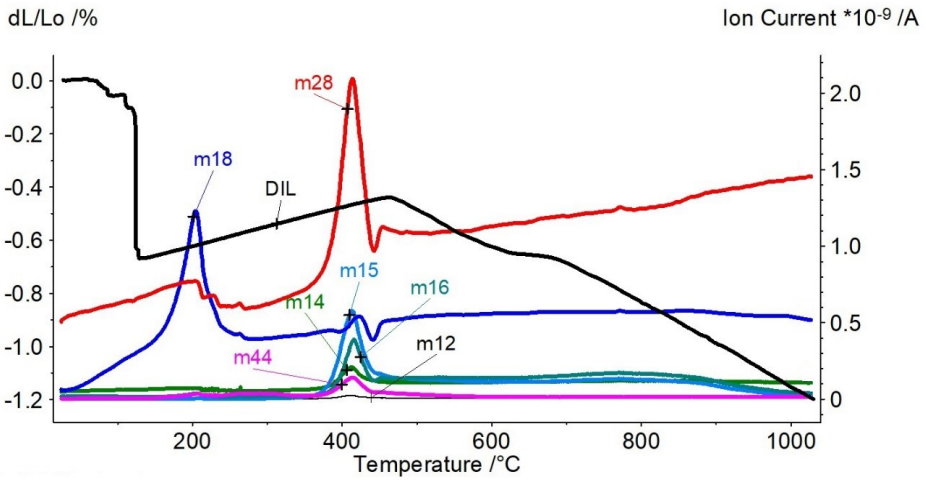

Fig.15. Mass spectrometry graphs of Cu sample, heating section of the dilatometric run.

Density, porosity and the amount of carbon and oxygen

The density measurement was partly not successful, because the wetting of the specimen by the displacement fluid (water) does not work sufficiently well on complex structures, air bubbles remaining and (erroneously) showing too high porosity. The theoretical density of Cu is about 8.96 g/cm3. The porosity was calculated from the theoretical density and the measured one. The results are shown in Tab..

Tab.7. Density and porosity of copper specimens.

Sample	Density [g/cm^3]	Porosity [%]
V3 (Filament)	7.47	16,6
Sample 2	7.24	19,2

The filament V3 shows less porosity than sample 2, which is clear because sample 2 has much more interspaces than the filament that trap air bubbles. Thus, the recorded density of the filament V3 is higher than that of sample 2.

The carbon content and the oxygen content were also measured on the samples V2, V3, Sample and Sample 2. The results are summarized in Tab..

Tab.8. Carbon and oxygen content of copper specimens.

Sample	Carbon [*µg/g*]	Oxygen [*µg/g]*
V2	50 ± 16	128 ± 21
V3	419 ± 48	230 ± 17
Sample 1	49 ± 7	80 ± 23
Sample 2	29 ± 9	164 ± 63

All samples have a very low carbon and oxygen content, with the sample V3 (filament) having the highest carbon content of 419 µg/g. The other samples have a low carbon content (approx. 30 to 50 µg/g). The oxygen content of all samples is higher than the carbon content, but still relatively low, with sample V3 again having the highest oxygen content (230 µg/g).

Light Microscopy

Light microscopy images show pores already that are visible in the unetched state and thus are fairly coarse porosity. It is possible that this porosity already originates from inhomogeneities in the starting material and is enhanced by the sintering process, through Ostwald ripening of the pores, i.e. growth of larger pores at the expense of finer ones [47].

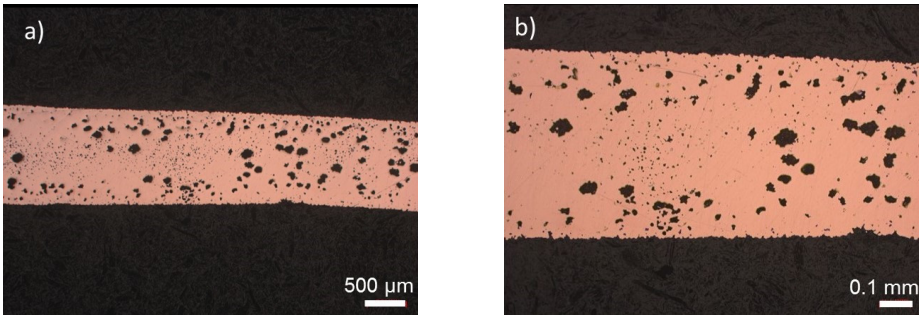

Fig.16. LO micrographs of unetched sintered sample V3 (filament). 25x (a) and 50x (b).

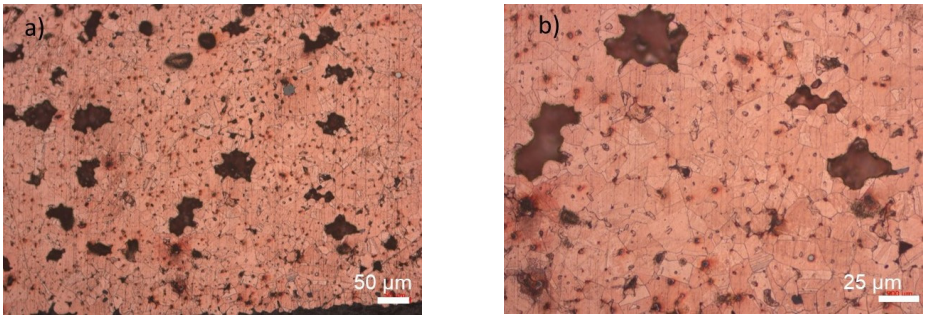

Fig.17. LO micrographs of etched sintered sample V3 (filament), 100x (a) and 200x (b). The etching was carried out by a Heyn-agent.

CONCLUSIONS

Use of steel feedstock for the manufacturing of components

Debinding with cyclohexane worked well, although care must be taken with flat components to avoid deformation. The weight loss is approx. 5.7 %. The sample E1 stands in a bed of coarse corundum particles during sintering, whereby the shrinkage at the bottom of the tested sample was not the same as on the top. Therefore, one should sinter horizontally or alternatively use a fixed alumina layer (flat, smooth plate). Sintering at 1350°C under hydrogen atmosphere resulted in a good densification in any case, and also the carbon content after sintering is very low.

Use of copper feedstock for the production of components

Debinding has been successful so far, but the parts already become relatively soft at 80°C. The loss of mass during solvent debinding was approx. 5 % for each sample. In the next step, the samples can be sintered quite well in a humid hydrogen atmosphere. This solves the problem of residual carbon impurities and, consequently, the final C content and also the oxygen content are very low. The deformation of the specimen takes place relatively early, which has been proved by dilatometry and mass spectrometry. At about 124°C, the backbone polyethylene already melts, resulting in a loss of structural strength. At 400°C, the residual organic binder is removed, which is mainly visible by appearance of carbon-containing fragments in the mass spectrometer. The main problem here is the distortion of larger specimens in the early stage of sintering; this should be overcome by using a backbone binder component with significantly higher melting range that remains mechanically stable up to temperatures at which bonds between Cu particles are already formed. This will be the topic of a subsequent publication.

Comparison of the sintering behaviour and characteristics of the materials

The comparison of the sintering behaviour of the steel and copper samples shows that both types can be sintered very well. Steel is sintered at markedly higher temperatures (1350°C) than copper (1060°C) in hydrogen. The measured density for the steel samples are 7.39 g/cm^3 (E1), 7.44 gm/cm^3 (E3) and 7.24 g/cm^3 (theoretical density: 8.00 g/cm^3) and the porosity calculated from this is 7.64 % (E1), 6.95 % (E3) and 9.49 g/cm^3. For the copper samples, the measured densities are between 7.2 and 7.5 g/cm^3 (theoretical density: 8.96 g/cm^3), with the resulting porosity being between 16 and 19 %, which is considerably higher than for the steel samples. However, density measurement is very difficult for the

complex copper samples studied here due to poor wetting of the structures and trapping of air bubbles. Also the addition of a wetting agent did not result in complete wetting of the copper samples with water, which means that the Archimedes method seems to be hardly suitable for these samples due to the very complex component geometry compared to the steel samples. The density measurement worked best for the copper samples with filament V3 due to the sample geometry of the filament. The porosity value of 16.6 % of V3 can therefore be considered relatively reliable. The carbon content of all samples is very low and therefore (as well as the oxygen content) does not influence the sintering significantly. The microstructures of the copper samples already showed a high porosity, most probably due to inhomogeneities in the feedstock. In the case of steel, larger pores were found due to the printing process, which must be prevented during printing. However, the fine pores found can hardly be avoided by solid state sintering. In any case, unwelcome reactions between the organic binder and the steel can be suppressed, carbide-free austenitic stainless steel being obtained.

Acknowledgement

This work was performed as part of the European projects REProMag and CerAMfacturing and the Austria-China bilateral cooperation project FlexiFactory3Dp. Both European projects have received funding from the European Union's Horizon 2020 research and innovation program under Grant Agreements No. 636881 and No. 678503. FlexiFactory3Dp has received funding from the Austrian Research Promotion Agency under the program Production of the Future, Grant Agreement No. 860385.

REFERENCES

[1] Gonzalez-Gutierrez, J., Cano, S., Schuschnigg, S., Kukla, C., Sapkota, J., Holzer, C.: Materials, vol. 11, 2018, doi:10.3390/ma11050840
[2] German, RM., Bose, A.: Injection molding of metals and ceramics. Princeton NJ : MPIF, 1997
[3] Chacón, JM., Caminero, MA., García-Plaza, E., Núñez, PJ.: Materials & Design, vol. 124, 2017, p. 143, doi:10.1016/j.matdes.2017.03.065
[4] Heller, BP., Smith, DE., Jack, DA.In: Proceedings of the Solid Freeform Fabrication Symposium. Austin, Texas, 2015
[5] Kuo, C-C., Mao, R-C.: Materials and Manufacturing Processes, vol. 31, 2015, p. 1113, doi:10.1080/10426914.2015.1090594
[6] Ahn, SH., Montero, M., Odell, D., Roundy, S., Wright, PK.: Rapid Prototyping Journal, vol. 8, 2002, p. 248, doi:10.1108/13552540210441166
[7] Alafaghani, A., Qattawi, A., Alrawi, B., Guzman, A.: Procedia Manufacturing, vol. 10, 2017, p. 791, doi:10.1016/j.promfg.2017.07.079
[8] Álvarez, K., Lagos, RF., Aizpun, M.: Ing. Inv., vol. 36, 2016, p. 110, doi:10.15446/ing.investig.v36n3.56610
[9] Bellehumeur, C., Li, L., Sun, Q., Gu, P.: Journal of Manufacturing Processes, vol. 6, 2004, p. 170, doi:10.1016/S1526-6125(04)70071-7
[10] Carneiro, OS., Silva, AF., Gomes, R.: Materials & Design, vol. 83, 2015, p. 768, doi:10.1016/j.matdes.2015.06.053
[11] Elkins, K., Nordby, H., Janak, C., Gray, RW., Bøhn, HH., Baird, DG. In: Proc. 8th. Solid Freeform Fabrication Symposium. The University of Texas, Austin, August 11-13 1997, p. 441
[12] Rahim, TNAT., Abdullah, AM., Akil, H., Mohamad, D., Rajion, ZA.: Express Polym. Lett., vol. 11, 2017, p. 963, doi:10.3144/expresspolymlett.2017.92

[13] Shojib Hossain, M., Espalin, D., Ramos, J., Perez, M., Wicker, R.: J. Manuf. Sci. Eng., vol. 136, 2014, p. 61002, doi:10.1115/1.4028538
[14] Masood, SH., Song, WQ.: Materials & Design, vol. 25, 2004, p. 587, doi:10.1016/j.matdes.2004.02.009
[15] Giberti, H., Strano, M., Annoni, M., Yuan, Y., Menon, L., Xu, X.: MATEC Web of Conferences, vol. 43, 2016, p. 3003, doi:10.1051/matecconf/20164303003
[16] Mireles, J., Espalin, D., Roberson, D., Zinniel, B., Medina, F., Wicker, R. In: Proceedings of the Solid Freeform Fabrication Symposium. Solid Freeform Fabrication Symposium. Austin, Texas, 2012, p. 836
[17] Venkataraman, N., Rangarajan, S., Matthewson, MJ., Safari, A., Danforth, SC., Yardimci, A., Guceri, SI. In: Proceedings of the Solid Freeform Fabrication Symposium. Solid Freeform Fabrication Symposium. Austin, Texas, 9-11 August, 1999
[18] Wu, G., Langrana, NA., Rangarajan, S., McCuiston, R., Sadanji, R., Danforth, SC., Safari, A. In: Proceedings of the Solid Freeform Fabrication Symposium. Solid Freeform Fabrication Symposium. Austin, Texas, 9-11 August, 1999, p. 775
[19] Wu, G., Langrana, NA., Sadanji, R., Danforth, S.: Materials & Design, vol. 23, 2002, p. 97, doi:10.1016/S0261-3069(01)00079-6
[20] Bandyopadhyay, A., Panda, RK., Janas, VF., Agarwala, MK., Danforth, SC., Safari, A.: Journal of the American Ceramic Society, vol. 80, 1997, p. 1366
[21] McNulty, TF., Mohammadi, F., Bandyopadhyay, A., Shanefield, DJ., Danforth, SC., Safari, A.: Rapid Prototyping Journal, vol. 4, 1998, p. 144, doi:10.1108/13552549810239012
[22] Venkataraman, N., Rangarajan, S., Matthewson, MJ., Harper, B., Safari, A., Danforth, SC., Wu, G., Langrana, N., Guceri, SI., Yardimci, A.: Rapid Prototyping Journal, vol. 6, 2000, p. 244, doi:10.1108/13552540010373344
[23] Agarwala, MK., Weeren, R. van, Bandyopadhyay, A., Safari, A., Danforth, SC., Priedeman, WR. In: Proceedings of the Solid Freeform Fabrication Symposium. Solid Freeform Fabrication Symposium. Austin, Texas. Eds. DL. Bourell, et al., 1996
[24] Agarwala, MK., Weeren, R. van, Bandyopadhyay, A., Whalen, PJ., Safari, A., Danforth, SC. In: Proceedings of the Solid Freeform Fabrication Symposium. Solid Freeform Fabrication Symposium. Austin, Texas. Eds. DL. Bourell, et al., 1996
[25] Agarwala, MK., Jamalabad, VR., Langrana, NA., Safari, A., Whalen, PJ., Danforth, SC.: Rapid Prototyping Journal, vol. 2, 1996, p. 4, doi:10.1108/13552549610732034
[26] Allahverdi, M., Danforth, SC., Jafari, MA., Safari, A.: Journal of the European Ceramic Society, vol. 21, 2001, p. 1485, doi:10.1080/00150190108225177
[27] Atisivan, R., Bose, S., Bandyopadhyay, A.: Journal of the American Ceramic Society, vol. 84, 2001, p. 221, doi:10.1111/j.1151-2916.2001.tb00635.x
[28] Bandyopadhyay, A., Das, K., Marusich, J., Onagoruwa, S.: Rapid Prototyping Journal, vol. 12, 2006, p. 121, doi:10.1108/13552540610670690
[29] Iyer, S., McIntosh, J., Bandyopadhyay, A., Langrana, N., Safari, A., Danforth, SC., Clancy, RB., Gasdaska, C., Whalen, PJ.: Int J Applied Ceramic Technology, vol. 5, 2008, p. 127, doi:10.1111/j.1744-7402.2008.02193.x
[30] Jafari, MA., Han, W., Mohammadi, F., Safari, A., Danforth, SC., Langrana, N.: Rapid Prototyping Journal, vol. 6, 2000, p. 161, doi:10.1108/13552540010337047
[31] McNulty, TF., Shanefield, DJ., Danforth, SC., Safari, A.: Journal of the American Ceramic Society, vol. 82, 1999, p. 1757, doi:10.1111/j.1151-2916.1999.tb01996.x
[32] Pistor, CM.: Adv. Eng. Mater., vol. 3, 2001, p. 418, doi:10.1002/1527-2648(200106)3:6<418:AID-ADEM418>3.0.CO;2-Q

[33] Rangarajan, S., Qi, G., Venkataraman, N., Safari, A., Danforth, SC.: Journal of the American Ceramic Society, vol. 83, 2000, p. 1663, doi:10.1111/j.1151-2916.2000.tb01446.x
[34] Lengauer, W., Duretek, I., Schwarz, V., Kukla, C., Kitzmantel, M., Neubauer, E., Lieberwirth, C., Morrison, V. In: Euro PM2018 Proceedings. EURO PM2018 Congress & Exhibition. Bilbao, Spain, 14. - 18. October. Bellstone : EPMA, 2018 p. 1
[35] Bai, Y., Williams, CB.: Rapid Prototyping Journal, vol. 21, 2015, p. 177, doi:10.1108/RPJ-12-2014-0180
[36] Hwang, KS., Hsieh, YM.: Metall Mater Trans A, vol. 27, 1996, p. 245, doi.org/10.1007/BF02648403
[37] Danninger, H., Frauendienst, G., Streb, K., Ratzi, R.: Dissolution of different graphite grades during sintering of PM steels, 2001, 67, p. 72
[38] Danninger, H., Gierl, C.: Processes in PM steel compacts during the initial stages of sintering, 2001, 67, p. 49
[39] Danninger, H., Gierl, C., Kremel, S., et al.: Degassing and deoxidation processes during sintering of unalloyed and alloeyd pm stells, 2002, 2, p. 125
[40] Azadbeh, M., Danninger, H., Gierl-Mayer, C.: Particle rearrangement during liquid phase sintering of Cu – 20Zn and Cu – 10Sn – 10Pb prepared from prealloyed powder, 2013, 56, p. 2, doi.org/10.1179/0032589913Z.000000000138
[41] Oro Calderon, R. de, Campos, M., Gierl-Mayer, C., Danninger, H., Torralba, JM.: Metallurgical and Materials Transactions A, vol. 46, 2015, p. 1349
[42] Butković, S., Oruč, M., Šarić, E., Mehmedović, M.: Mater Tehnol, vol. 46, 2012, p. 185
[43] Slotwinski, JA., Garboczi, EJ., Hebenstreit, KM.: J Res Natl Inst Stand Technol, vol. 119, 2014, p. 494, doi.org/10.6028/jres.119.019
[44] Hairer, F., Karelova, A.: Etching techniques for the microstructural characterization of complex phase steels by light microscopy, 2008, p. 50
[45] Gierl, C., Danninger, H., Avakemian, A., Synek, J., Sattler, J., Zlatkov, BS., Maat, J., Arzl, A., Neubing, HC.: Powder Injection Moulding International, vol. 6, 2012, no. 4, p. 65
[46] Zlatkov, BS., Griesmayer, E., Loibl, H., Aleksić, OS., Danninger, H., Gierl, C., Lukić, LS.: Science of Sintering, vol. 40, 2008, p. 79, https://doi.org/10.2298/SOS0801077Z
[47] Schatt, W.: Sintervorgänge. Düsseldorf : VDI-Verlag, 1992

sciendo
Powder Metallurgy Progress, Vol.19 (2019), No.2, p.082-089
http://dx.doi.org/10.1515/pmp-2019-0008

PREPARATION, MICROSTRUCTURE EVALUATION AND PERFORMANCE ANALYSIS OF DIAMOND-IRON BONDED MAGNETIC ABRASIVE POWDER

Palwinder Singh, Lakhvir Singh, Sehijpal Singh

Abstract

The customary edged tool for machining is uneconomical for harder and hard to machine materials and furthermore the level of surface finish accomplished is not that great. As of late, a lot of consideration in mechanical engineering has been centered on finishing tasks. Not many investigations have been accounted for till date on the advancement of substitute magnetic abrasive powder (MAP). In this paper, to improve the finishing performance, the abrasive powder were prepared by mechanical alloying of diamond powder and iron (Fe) powder, compacting these with universal testing machine (UTM) and then sintered at different temperature in a sintering machine in an inert gas (H2) atmosphere. These compacts were crushed and sieved to obtain various sizes of MAP. This abrasive powder were micro-structurally examined. The results indicate that the densification increases and porosity decreases with increasing temperature. Moreover, the prepared bonded MAP has potential performance as a new MAP for fine finishing in Magnetic Abrasive Flow Machining (MAFM) process.

Keywords: mechanical alloying, sintered, magnetic abrasive powder, diamond, Universal Testing Machine (UTM), bonded, Magnetic Abrasive Flow Machining (MAFM)

INTRODUCTION

There has been a quick development in the advancement of difficult and hard to machine materials and alloys during the most recent two decades. The standard edged tool machining is costly for these kind of materials and level of surface finish feasible is poor. As of late, a lot of consideration in mechanical engineering has been centered around finishing tasks went for fixing the finishing tolerance of machined segments. It is hard to finish propelled engineering materials with high exactness, and negligible surface imperfections, for example, small scale splits, by traditional grinding and cleaning procedures. To limit the surface harm, delicate adaptable finishing conditions are desirable, in particular, a low degree of controlled power. Magnetically assisted manufacturing processes are getting to be powerful in finishing, cleaning, deburring and shining of metal and propelled engineering material components. In perspective on the reality of this issue, as of late new unconventional fine machining techniques like Magnetic Float Machining (MFM), Magnetic Abrasive Polishing, Magnetic Abrasive Finishing (MAF) and Magnetic Abrasive Flow Machining (MAFM) have been developed.

Palwinder Singh: Research Scholar, IKGPTU, Kapurthala, India
Lakhvir Singh: Mech. Engg. Department, BBSB Engg. College, Fatehgarh Sahib, India
Sehijpal Singh: Mech. Engg. Department, Guru Nanak Dev Engg. College, Ludhiana, India

Most of the existing studies throw light on the development of process and in the direction of enhancing the capabilities and applications of the process. However, the major constraint in wide spread adoption of this technology is the exorbitant cost of magnetic abrasives, which acts as a cutting tool in MAFM, not many investigations have been accounted for till date on the advancement of substitute magnetic abrasive powder.

Amir D. et al. [1] used unbonded SiC abrasives based media for the finishing of biomedical devices of stainless Steel 304. They reported that with increased MFD, the surface finish reduces. Also a fine surface finish was obtained with increased mesh number. Bahre et al. [2] employed AFM for machining of high strength steel AISI 4140 using Al2O3 abrasive based media and reported that higher piston pressure resulted in required surface finish. Butola et al. [3] investigated AFM process optimization for finishing of aluminum tube. The aluminum tube was finished by Al_2O_3, SiC and B_4C abrasives based media. Khairy [4] prepared magnetic abrasive particles by blending of Al_2O_3 and Fe powders (85%) compacting them, sintered the mixture in a furnace at 1400° C in inert atmosphere, crushing into small particles and sieving to obtain different sizes. Kreman et al. [5] developed magnetic abrasives by using the technique in which an adhesive is used to bind magnetic iron powder with Al_2O_3 powder. All the constituents were mixed, dried and crushed into small desired sizes for machining. Lin et al. [6] prepared magnetic abrasives by typically mixing Fe powder and Al_2O_3, compressed, sintered and crushed to produce average size 150 micrometer. Shinmura et al. [7] prepared two kinds of magnetic abrasives. The particle size of Fe in one and the particle size of abrasive particle in other was changed. The abrasive particle size affected stock removal comparatively less while surface roughness was significantly affected while iron particle size significantly affected both stock removal and surface finish. Singh and Shan [8] machined brass material by Brown Super Emery as magnetic abrasives to evaluate the performance of MAFM process. Sankar et al. [9] finished Al alloy based metal matrix composites (MMCs) by unbonded SiC abrasive particles in abrasive medium. They reported that Al alloy/SIC (10%) MMC had better Ra amongst three workpiece materials. Sran et al. [10] prepared mechanically alloyed magnetic abrasives for finishing of brass tubes up to 3 nm level. Singh et al. [11] reported that annealing temperature effects the magnetic properties of the magnetic abrasives. It was reported that annealing/sintering temperature of 950°C resulted in a maximum value of MFD. Yamaguchi et al. [12] developed spherical Fe based magnetic abrasive containing Al_2O_3 abrasives made by plasma spray technique. As the literature shows that most of the researchers had used unbonded abrasive particles in abrasive laden media for AFM or MAFM process. So preparation and performance evaluation of bonded magnetic abrasive powder in abrasive laden media needed to be investigated.

EXPERIMENTAL DETAILS

Experimental set up for preparing magnetic abrasive powder

The external photograph and schematic view of sintering machine is shown in Fig. 1 and Fig. 2 respectively. Sintering machine is an electric furnace in which specially designed stainless steel tube is used. The specimens of magnetic abrasive powder are placed in this tube and heated at given temperature ranges for 2 hours. Simultaneously H_2 gas is passed through tube to create inert atmosphere. The main parts of sintering machine are:

a) Electric Furnace (Max 1200° C)
b) Thermocouple
c) Stainless Steel (AISI 310S) Tube

d) Power Supply & Control Unit of the Furnace
e) H2 Gas Cylinder
f) Pressure Regulator & Pressure Gauges

Fig.1. External view of sintering machine.

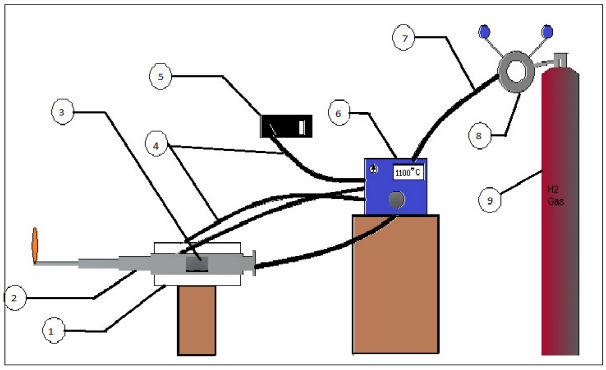

Fig. 2. Schematic view of sintering machine: 1. Furnace; 2. Stainless Steel (AISI 310) Tube; 3. Specimens for Sintering; 4.Power Cable; 5. Main Supply 220v; 6. Power Supply & Control Unit of Furnace; 7. Hose Pipe for H_2 Gas; 8. Pressure Regulator and Pressure Gauges; 9. H_2 Gas Cylinder.

Preparation of sintered magnetic abrasive powder

The following procedure was adopted for the preparation of sintered magnetic abrasive powder:

- ❖ Mixing and mechanical alloying of Fe and diamond powders
- ❖ Preparing the compacts
- ❖ Sintering of compacts

Crushing of compacts and sieving

Mixing and mechanical alloying of iron and diamond powders

The Fe powder and (300 mesh size) and diamond powder (270 mesh size) powders were mixed thoroughly in 70%Fe+30%diamond proportion by volume percentage. This mixing was followed by mechanical alloying technique in which the powder particles were exposed to affect by high strength stainless steel balls in a ball mill/attritor at room temperature. After the process, very small MAPs are obtained in which the abrasive particles are connected to the base metal grid with no holding material.

Preparation of compacts

The compacts of Fe + diamond were prepared in cylindrical die by using Universal Testing Machine (UTM) in this work as shown in Fig. 3. The mixtures that is used here is mixed by the volume percentage i.e. 70% Fe and 30% diamond proportion.

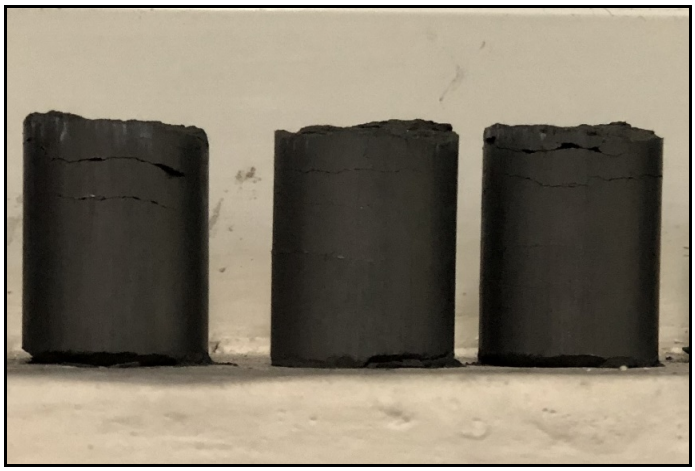

Fig.3. Compacts of mechanically alloyed magnetic abrasive powder.

Sintering of compacts

The compacts were placed within the stainless steel tube and were heated with the help of an electric furnace at temperature of 850°C, 950°C and 1050°C. The furnace raised the temperature of the specimens up to 1050°C and simultaneously the H_2 gas was supplied through hose pipe with suitable pressure that was indicated by the pressure gauges attached on the cylinder containing H_2 gas for two hours. The pressure was controlled by pressure regulator. At last the furnace was switched off and sintering specimens were cooled at a very slow rate to refine the structure of the specimens. The hydrogen gas helps to produce improved surface crystalline, eliminates scaling, achieves optimum magnetic characteristics, and removes impurities like surface carbon, phosphorous. A nomenclature was given to three samples i.e. 30DFe850, 30DFe950 and 30DFe1050. Here 30D denotes percentage of diamond in iron, Fe denotes iron and 850, 950 & 1050 are the sintering temperatures. The sintered compacts are shown in Fig. 4.

Fig.4. Sintered compacts.

Crushing of compacts and sieving

The sintered compacts were crushed mechanically into desired size. The sintered compacts were crushed into powder form. Then powdered abrasives were passed through different sieves to get different abrasive sizes. The obtained abrasive sizes were 200, 275 and 350 mesh size.

RESULTS AND DISCUSSION

Microstructure evaluation of prepared bonded magnetic abrasive powder

To examine the sintering improvement of phase and microstructure, micrographs of the prepared magnetic abrasive powder was recorded utilizing scanning electron microscopy (SEM). The microstructure photographs of all the specimens' shows three types of grains, white ones are of diamond, black are of Fe and greyish are of Fe+diamond. The nano size particles of Fe+diamond were formed. The Fe+diamond formed in this case is due to reactive sintering between diamond and Fe particles. The various particles, i.e. of Fe, diamond and iron+diamond, present in the microstructure have been marked on the photographs.

Figure 5 shows the microstructure of It can be clearly seen that with increase in temperature dense phase formation increases and porosity decreases. The specimen 30DFe1050 is denser in comparison to specimen 30DFe950 and 30DFe850.

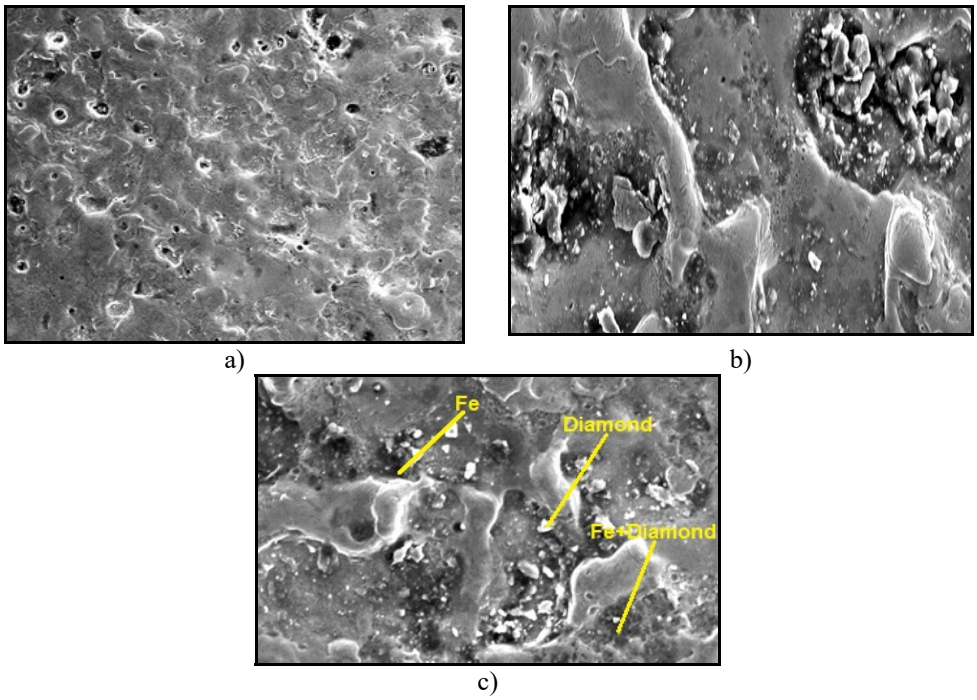

Fig.5. Microstructure photos of a) 30DFe850, b) 30DFe950 and c) 30DFe1050.

Performance analysis of prepared bonded magnetic abrasive powder

The performance of prepared magnetic abrasive powder was evaluated in terms of SRIR (Surface Roughness improvement Rate) and MRR (material removal rate). The internal finishing of aluminum tubes was performed on magnetic abrasive flow machining (MAFM) set up (Fig. 6) using the prepared magnetic abrasive powder. The constant parameters were taken as 0.6 Tesla MFD (Magnetic Flux Density), 4.2 MPa extrusion pressure, 20 no. of cycles for evaluation. The work specimen to be machined/finished internally is hydraulically clamped in between the two media cylinders. Further two media cylinders are there in which the piston reciprocates by the motion of the hydraulic cylinders. The developed magnetic abrasive powder was mixed to form abrasive laden media, is filled in the lower chamber and then it is moved in the upward direction by the reciprocating drive given to the media cylinder piston. After completing the upward stroke the DC valve will operate in the other direction and the pistons will start coming downward, by pushing the media in the downward direction against the restrictions in the geometry of the fixtures to obtain the required pressure for abrasion to get finer finishing in the work piece.

As it can be clearly seen from the Fig. 7, that SRIR and MRR are higher at sintering temperature of 950°C. The possible reason could be that the MFD was found to have highest effect at 950°C of annealing/sintering temperature [11]. Therefore, the prepared bonded magnetic abrasive powder has potential performance as a new magnetic abrasive powder for fine finishing.

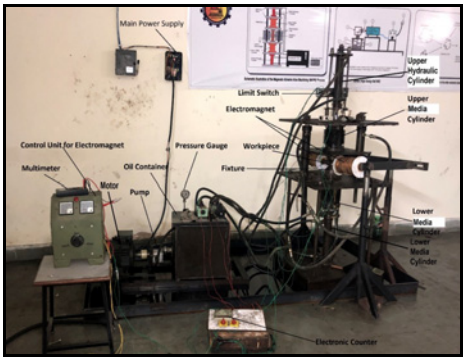

Fig.6. MAFM set up.

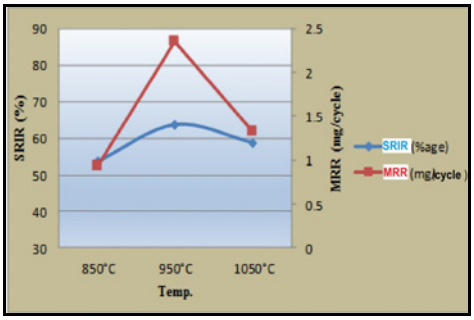

Fig. 7. Effect of sintering temperature on SRIR and MRR.

CONCLUSIONS

The conclusions drawn from this research work are summarized as follows:

1. The mechanical alloying followed by sintering of magnetic abrasive powder results in induced ductility, relieves internal stresses, refines the structure and increases the bonding strength of diamond + Fe abrasive powder.
2. The dense phase formation increases and porosity decreases with increase in sintering temperature.
3. The prepared bonded magnetic abrasive powder has potential performance as a new magnetic abrasive for fine finishing. The magnetic abrasive powder 30DFe950 delivered higher surface roughness improvement.

Acknowledgement

We hereby express our heartfelt thanks to department of RIC, IKGPTU and BBSBEC College for their continuous support.

REFERENCES

[1] Amir, D., Behzad, F., Behrouz, M., Navid, N.: Research and Development in Material Science, vol. 8, 2018, p. 1
[2] Bahre, D., Brunnet, H., Swat, M.: 5th CIRP Conf. High Performance Cutting, Procedia CIRP, vol. 1, 2012, p. 419
[3] Butola, R., Jain, R., Bhangadia, P., Bandhu, A., Walia, R.S., Murtaza Q.: Materials Today, Proceedings, vol. 5, 2018, p. 4720

[4] Khairy, AB.: Journal of Materials Processing Technology, vol. 116, 2001, p. 77
[5] Kreman, G., Elsayed, E., Feygin, S., Lgelshteyn, L. In: Proceeding of International Machining and Grinding Conference. Vol. 3. Cincinnati, Ohio, 1999
[6] Lin, C., Tein, Y., Lieh, D., Chow, HM.: International Journal of Advance Manufacturing Technology, vol. 34, 2007, p. 122
[7] Shinmura, T., Takazawa, K., Hatano, E., Matsunaga, M.: Annals of the CIRP, vol. 39, 1990, p. 325
[8] Singh, S., Shan, HS.: International Journal of Machine Tools and Manufacture, vol. 42, 2002, p. 953
[9] Sankar, MR., Ramkumar J., Jain, VK.: Wear, vol. 266, 2009, p. 688
[10] Sran, LS., Khangura, SS., Singh, A. In: Proceeding of the ASME International Manufacturing Science and Engineering Conference. Notre Dame, Indiana, USA, 2012
[11] Singh, A., Singh, S., Singh, L.: International Journal of Advanced in Management, Technology and Engineering Sciences, vol. 7, 2017, no. 11, p. 246
[12] Yamaguchi, H., Kataro, H. (2008). Journal of Manufacturing Science and Engineering, vol. 130, 2008, p. 031107-1

sciendo
Powder Metallurgy Progress, Vol.19 (2019), No.2, p.090-096
http://dx.doi.org/10.1515/pmp-2019-0009

EXPERIMENTAL INVESTIGATIONS ON IMPACT TOUGHNESS AND SHEAR STRENGTH OF NOVEL LEAD FREE SOLDER ALLOY Sn-1Cu-1Ni-XAg

Jayesh S, Jacob Elias

Abstract
Lead is known to be banned in alloy making, highlighting toxicity concerns and environmental legislations. Researchers and scholars around the globe were in immediate search of new lead free solder alloys which could potentially replace the old Sn-Pb alloy. In this comprehensive study, shear strength and impact toughness tests were conducted on Sn-1Cu-1Ni when different amounts of Ag (0.25, 0.5, 0.75 1 % by wt.) is added. Shear strength test is tested using micro force test system. Impact toughness test is analyzed using Charpy impact test set up by calculating the energy difference before and after impact. The study reveals that, Ultimate shear stress increased from 19 MPa to 21.3 MPa. Yield strength increased from 27.4 MPa to 29.7 Mpa. Impact toughness of the alloys increased from 9.4 J to 10.1 J. Thus, Sn-1Cu-1Ni-1Ag is found to have improved shear strength and impact toughness than Sn-1Cu-1Ni.
Keywords: solder alloy; lead free; impact toughness; shear strength

INTRODUCTION

Soldering basically is a metallurgical joining process which is done without melting the parent metals. The solder alloy in the molten liquid form will wet the surface of the parent metals, thereafter resulting in a bond formation between the work pieces once solidification sets [1]. In electronics packaging industry, the electronic components are soldered onto the printed circuit board (PCB) using the solder alloy. Therefore the solder alloy acts as a connection device between the electronics components and the circuit on the PCB [2]. Product reliability, mechanical properties, electrical properties, cost of the solder alloy etc. are some vital inputs that involve significant analysis. The failure of the solder alloy can lead to the failure of the functioning of the electronic package which may in turn make the device useless as a whole [3]. Electronic packages are used all round the world, especially in mobile industries, laptop industries, avionic industries, marine electronics etc. Hence, reliability of the solder alloy holds high significance. Sn-Pb alloy has improved properties like low melting point (183°C), good wettability on Cu, good hardness, good ductility, good workability, good availability, low cost etc. Due to the inherent toxicity of lead, the usage of lead has been banned from alloy making. Environmental legislations like RoHS (Restrictions on Hazardous Substance), WEEE (Waste Electrical and Electronic Equipment) sought the ban of Lead in electronic packages.

Jayesh S: Department of Mechanical Engineering, School of Engineering, Cochin University of Science and Technology, Kerala, India
Jacob Elias: Department of Mechanical Engineering, School of Engineering, Cochin University of Science and Technology, Kerala, India

Following this many countries also followed the legislations [4]. This led to the necessity of the need for new lead-free solder alloys which can replace the Sn-Pb solder alloy. Infact, the toxic nature of lead is not the only reason for search for lead-free solder joints. As the transistor density increases the solder joint pattern also changes. The pitch of this solder arrangement will be in trouble if Sn-Pb solder alloy is used in dense electronic packages. Behavior of customer and economy is yet another reason. Another reason is the need for high temperature solder alloys.

Research teams have started developing new lead free solder alloy which can be used as a replacement for the Sn-Pb alloy. Sn-Ag-Cu is found to alloy better with good properties. SAC105, SAC305, SAC405 are some examples. But the amount of Ag in SAC alloys will add to the cost. Besides the element costs, high patent costs also result. Many compositions were discovered as a replacement for Sn-Pb alloy. Some major compositions include Sn-Bi-Ag [5], Sn-Bi [6], Sn-Zn [7], Sn-Ag-Cu [8, 9], Sn-Cu [7], Sn-Zn-Bi [5]. The effect of addition of Ag into Sn-0.5Cu-1Bi (SCB305) and Sn-1Cu-1Ni (SCN110) were tracked, studied and the mechanical properties such as melting temperature, hardness and contact angle were found to be improved [10, 11]. Studies on the reliability under random vibrations were also studied [12]. The cost also was less when compared to the SAC alloys. In this paper, impact toughness and shear strength of the SCN110 are studied while Ag is added into it in 0.25, 0.5, 0.75, 1 % by wt.

EXPERIMENT

Sample preparation

Solder alloy specimens were intended and produced from pure metals which are in powder form. The composition and allocated codes are provided in the table 1. Powder form of pure metals of Sn, Cu, Ni and Ag are initially weighed in proper weight proportions. These were melted in induction furnace at more than 900°C for 45 minutes. These were then transferred to cylindrical molds. Five samples were made using the above procedure. The samples were quenched and were kept at room temperature for one day. The first sample was made using Sn, Cu and Ni according to the composition shown in the Table 1. In the next four samples Ag is added in four different proportions (0.25, 0.5, 0.75, and 1 % by wt.). These samples were obtained in the form of disc shapes. The samples are then undergone through visual inspection to ensure that the surface of these samples were free from damages[11].

Shear strength

The samples were produced as discussed in the sample preparation section. Five samples of each alloy were tested in the similar condition. For shear test to be conducted, micro lap shear solder joint samples were made. The same is shown in a schematic way in Figure 1 . All the five samplew set were ground using SiC paper, followed by polishing to eliminate any excess solder at the boundaries. Micro-force test system was used to conduct the shear strength test. A software was used to control the system. Test data are collected with the aid of this software. The shear strength tests were conducted on the five samples at room temperature. 5×10^{-4}/S is the strain rate used. The results were averaged among the five data.

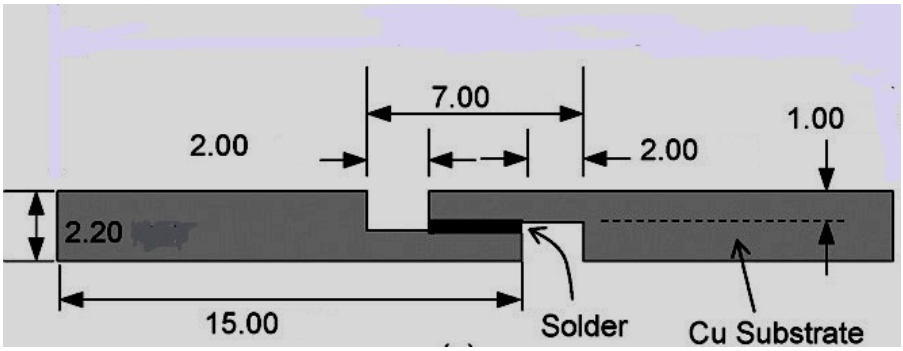

Fig.1. The samples for shear test.

Impact toughness test

In order to conduct the impact test, Charpy impact tests with pendulum type impact tester were used. The pendulum effective weight was 21Kg. Five specimens of each alloy were prepared with dimensions 70mm long x 5mm wide x 5mm thick. The schematic drawing given in the figure 2 shows the setup and the principle of the Charpy impact test. The pendulum is lifted to a height H. This is considered as the initial position. E1 is the initial potential energy. Then the pendulum is allowed to swing and hit the specimen. After hitting the specimen it rises to a height of H1. E2 is the energy at this stage and it is considered as the final energy. During hitting the specimen, some amount of energy E is absorbed by the specimen. The impact absorbed energy was obtained. The same procedure is repeated for all the five samples. The test data obtained is then averaged. The data regarding the absorbed energy obtained during the test helps in analyzing the impact toughness of the alloys.

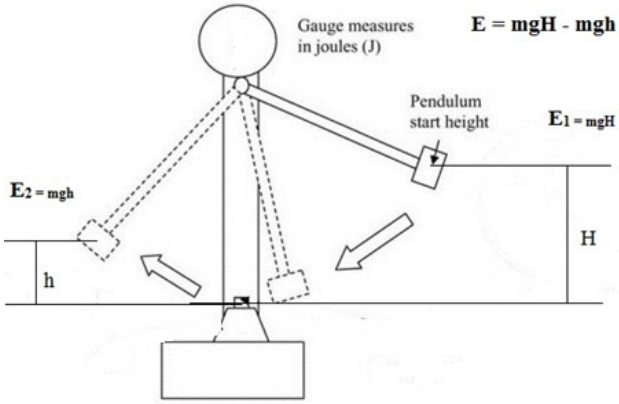

Fig.2. Impact toughness using Charpy apparatus (schematic representation).

Mechanical properties of the alloy

Mechanical properties of SCN110 alloy were tabulated [18]. Variations taking place while adding Ag in 0.25, 0.5, 0.75, 1 % by wt. were also investigated in the study. The melting temperature, contact angle and the hardness values are given in the table 1.

Tab.1. Melting temperature, contact angles and hardness of the alloys.

Solder Alloy	Melting Temperature [°C]	Contact angle [°]	Hardness [HV]
Sn-1Cu-1Ni	232.2	36.75	16.1
Sn-1Cu-1Ni-0.25Ag	231.2	27.54	16.3
Sn-1Cu-1Ni -0.5Ag	230.1	26.44	17.5
Sn-1Cu-1Ni -0.75Ag	229.4	24.12	18.7
Sn-1Cu-1Ni -1Ag	228.4	22.87	19.2

RESULTS AND DISCUSSION

Shear strength

Apart from the electrical properties, the mechanical properties of the solder alloys are very important, citing the fact that the electronic package should be reliable throughout its operational life. Material's ability to resist forces that can cause the internal structure of the material to slide against itself is termed as shear strength. Shear strength tests of the samples with different amount of Ag are conducted using the method explained in the above section. The results of the analysis are noted and are given in the table 2. Following strengthening mechanisms can be identified as the reason for improvement in the mechanical properties. Geometrically similar dislocations generated which accommodate the elastic modulus and thermal modulus mismatch. The results obtained are shown in the Figure 3. The dispersion hardening with the addition may be a reason for the increase in the shear strength. With the addition of Ag, the density of the alloy is also found to be increasing slightly. The ultimate shear stress of Sn-1Cu-1Ni is found to be increased by 8.3% by wt. with 1% addition of Ag.

Tab.2. Shear strength results of the alloys.

Solder Alloy	Ultimate Shear stress [MPa]	Yield Strength [Mpa]
Sn-1Cu-1Ni	27.4	19
Sn-1Cu-1Ni-0.25Ag	27.2	19.1
Sn-1Cu-1Ni -0.5Ag	28.3	20.4
Sn-1Cu-1Ni -0.75Ag	29.2	21.1
Sn-1Cu-1Ni -1Ag	29.7	21.3

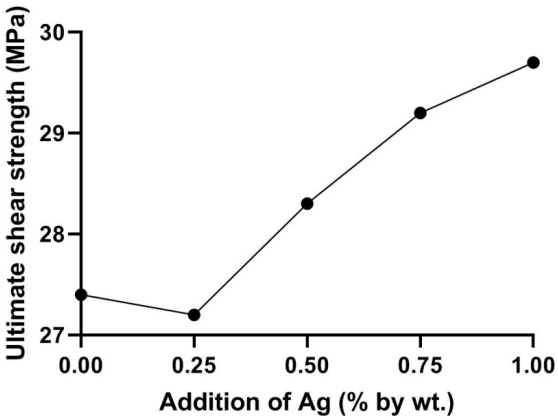

Fig.3. Ultimate shear strength of the alloys.

Impact toughness

Impact toughness is a fundamental material property required to measure the performance of solder alloys. The impact toughness is directly proportional to the energy absorbed by the alloy. The crashworthiness of the solder alloy is an important property. Impact strength can be defined as the measure of energy that a specimen can absorb during the conduction of the test before fracturing. During fracturing it undergoes rapid rate of deformation. Impact toughness tests for all the samples with different amount of Ag are conducted using charpy impact test explained in the previous section. The energy absorbed by the test specimen gives idea about the impact toughness. The results obtained are given in the table 3. The results obtained are shown in the figure 4.The samples which are able to absorb more impact energy during the conduction of impact test will be considered as materials having more impact toughness. The microstructure also will have close relation with the impact toughness. Charpy test is the apt test for determining the impact toughness of the solder alloy. Even if we are using large test specimens for the test when compared to the solder joints, the strain rate experiencing in the both cases are matching. The impact toughness of Sn-1Cu-1Ni is found to be increased by 3.1% with the addition of 1% by wt. Ag.

Tab.3. Impact toughness test results of the alloys.

Solder Alloy	Impact Toughness [J]
Sn-1Cu-1Ni	9.4
Sn-1Cu-1Ni-0.25Ag	9.7
Sn-1Cu-1Ni -0.5Ag	9.8
Sn-1Cu-1Ni -0.75Ag	9.9
Sn-1Cu-1Ni -1Ag	10.1

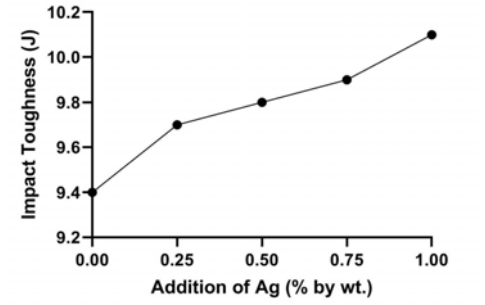

Fig.4. Impact toughness test results.

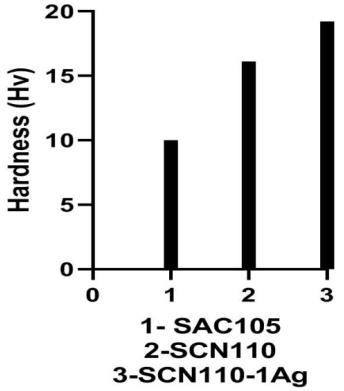

Fig.5. Hardness comparison.

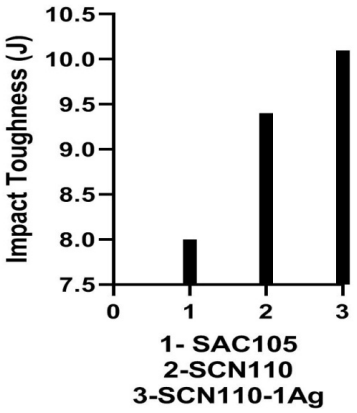

Fig.6. Impact toughness comparisons.

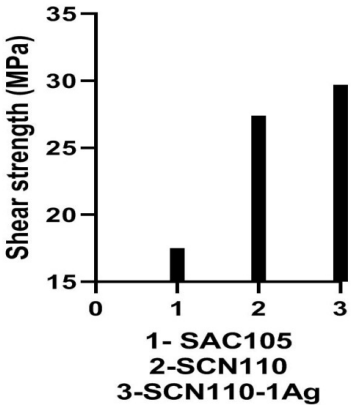

Fig.7. Shear strength comparisons.

CONCLUSION

The lead free solder alloys are prepared in the induction furnace where Sn, Cu, Ni and Ag are available in the form of powder. The chemical composition were verified. Shear strength test and impact toughness test were carried out first on Sn-1Cu-1Ni and then on Sn-1Cu-1Ni-xAg (x= 0.25, 0.5, 0.75, 1% by wt.) using micro force test system and Charpy impact testing apparatus. Ultimate shear stress is found to be increased from 19 MPa to 21.3 MPa. Yeild strength is found to be increased from 27.4 MPa to 29.7 MPa. The ultimate shear stress of Sn-1Cu-1Ni is found to be increased by 8.3% by wt. with 1% addition of Ag. This alloy (Sn-1Cu-1Ni-1Ag) is found to be having good mechanical properties (melting temperature, contact angle and hardness) with the addition of 1% of Ag. Impact toughness of the alloys increased from 9.4 J to 10.1 J. The impact toughness of Sn-1Cu-1Ni is found to be increased by 3.1% with the addition of 1% by wt. Ag. A comparison of hardness, shear strength and impact toughness between Sac105, SCN110, SCN110-1Ag is shown in the figure 5, figure 6 and figure 7. Sn-1Cu-1Ni-1Ag is found to be having good improved shear strength and impact toughness than Sn-1Cu-1Ni.

Acknowledgements

This research did not receive any specific grant from funding agencies in the public, commercial, or not-for-profit sectors.

REFERENCES

[1] Schwartz, MM.: Soldering: Understanding the basics. 1st edition. ASM International, USA, 2014
[2] Manko, HH.: Solder and Soldering. 2nd edition. New York : McGraw-Hill, 1979
[3] Cheng, S., Huang, C-M., Pecht, M.: A review of lead-free solders for electronics applications. Microelectronics Reliability, 2017, 10.1016/j.microrel.2017.06.016
[4] European Parliament. Proposal for a Directive of the European Parliament and of the Council on Waste Electrical and Electronic Equipment and on the restriction of the use of certain hazardous substances in electrical and electronic equipment. COM 2000;:347
[5] Gain, AK., Zhang, L.: J. Mater. Sci. Mater. Electron., vol. 27, 2016, p. 781
[6] Gain, AK., Chan, YC., Yung, KC., Sharif, A., Ali, L.: Mater. Sci. Eng. B, vol. 162, 2009, p. 92
[7] Chang, C., Chuang, TH., Feng, LP., Tsao, LC.: Mater. Des., vol. 32, 2011, p. 4720
[8] Leong, L., Fang, CJ., Chu, CP.: J. Mater. Sci. Mater. Electron., vol. 22, 2011, p. 1443
[9] Chen, S., Kaoa, CR.: J. Alloys Compd., vol. 520, 2012, p. 244
[10] Jayesh, S., Elias, J.: Met. Mater. Int., 2019, https://doi.org/10.1007/s12540-019-00305-3
[11] Elias, JSJ.: Lett. Mater., vol. 9, 2019, no. 2, p. 239
[12] Jayesh, S., Jacob, E.: Int. J. Simul. Multisci. Des. Optim., 10.1051/smdo/2019013